Prell, W. L., Niitsuma, N., et al., 1991
Proceedings of the Ocean Drilling Program, Scientific Results, Vol. 117

29. HIGH-RESOLUTION GEOCHEMICAL VARIATIONS AT SITES 723, 728, AND 731: A COMPARISON OF X-RAY FLUORESCENCE AND GEOCHEMICAL LOGS[1]

Richard D. Jarrard[2] and Mitchell Lyle[2]

ABSTRACT

Geochemical logging is a routine part of the Ocean Drilling Program, yet the reliability of ODP geochemical logs has rarely been evaluated quantitatively. On ODP Leg 117, geochemical logs were obtained at Sites 723, 728, and 731. We report here an evaluation of ODP geochemical log quality based on high-resolution sampling and X-ray fluorescence measurement of 398 core samples from the three sites.

At these sites we lacked the complete suite of high-quality logs needed for accurate log-based estimation of elemental percentages; only calcium and silicon logs had magnitudes similar to those from XRF. However, relative variations of log-based elemental abundances could be determined. Our comparisons of the XRF analyses with the character of variations in geochemical logs indicates that the reliability of ODP geochemical logs varies substantially, within short intervals and particularly between sites. In general, the geochemical logs are capable of detecting changes in formation geochemistry that are larger than the following thresholds: 2% for Ca, 2%–6% for Si, 0.5%–1% for K, 0.1% for Ti, 0.5% for Fe, and 0.4% for Al. All sulfur variations observed in the XRF data, as well as many of the iron variations, were below the resolving power of the geochemical logging tools. These precisions are generally similar to those determined at the Conoco test well by Chapman et al. (1987), in spite of the very different ODP logging conditions.

INTRODUCTION

The mineralogy of deep-sea sediments contains clues to the temporal variation of climate, depositional processes, and diagenesis. The geochemistry of deep-sea sediments reflects variations in this mineralogy. Some geochemical ratios such as Ti/Al can be directly interpreted in terms of changing source regions (e.g., Lyle et al., 1987), while calculation of normative mineralogy from geochemical data aids in determination of the geological significance of other geochemical variations (e.g., Herron, 1986). However, any geological interpretation of geochemical data is dubious, unless we have some idea of the precision and accuracy of these data.

Two primary types of geochemical data are available from the Ocean Drilling Program (ODP). First, major elements and some minor elements can be determined by X-ray fluorescence (XRF) analysis of small volumes of core (usually about 10 cm^3). Second, abundances of up to 13 elements (K, Th, U, Ca, Si, Fe, Mg, S, Al, Ti, Gd, Cl, and H) can be determined from geochemical logging.

The geochemical logs have several potential advantages over XRF analyses:

1. The logs are continuous over the entire logged interval, independent of the vagaries of core recovery and core disturbance;
2. The logs are representative, sampling a much larger volume than an XRF measurement and unaffected by preferential core recovery of certain lithologies in mixed lithology intervals;
3. Log data acquisition is very efficient (several hundred meters can be geochemically logged in the time required for only a few XRF measurements).

In comparison to XRF analyses, geochemical logs have two major disadvantages:

1. Some elements can be determined by XRF analysis that cannot be determined by logs;
2. The precision and accuracy of XRF analyses are well-determined and high, while the precision and accuracy of geochemical logs are poorly known.

This paper focusses on evaluation of the reliability of ODP geochemical logs, largely by comparison to XRF measurements. We analyze and compare geochemical logs and XRF measurements from three sites drilled on ODP Leg 117: Sites 723, 728, and 731. Sites 723 and 728 are on the Oman margin; Site 731 is on Owen Ridge. These sites were selected for study for several reasons:

1. Core recovery was unusually high at these sites, due to a combination of favorable lithologies for ODP core recovery, very calm seas during drilling, and relatively uniform and modest lithification. Sites 723 and 728 were double cored for further improvement of core recovery; however, we confine our analyses to only one hole per site, because detailed matching and correction of recovery depths between holes has not been undertaken yet for these sites.
2. Core disturbance was unusually low for the analyzed portions of these sites. All coring utilized the extended core barrel (XCB), and we have never seen XCB cores that exhibit less core disturbance than these. The core disturbance in general appears to be almost as low as with the advanced piston corer (APC); APC cores are less suitable for comparison to geochemical logs, because they are usually confined to the depth interval in which geochemical logs are obtained through pipe and therefore are less reliable than the openhole geochemical logs considered here.
3. Geochemical logs were obtained from all three sites. Though routine in ODP, geochemical logging is not ubiquitous. Unfortunately, the complete suite of geochemical logs was obtained only at Site 723, as described in a subsequent section.
4. Substantial geochemical variability occurs within each of the three sites, at a depth scale large enough to make individual XRF measurements representative and to avoid averaging of major geochemical variations by individual log measurements. This conclusion was based on visual core descriptions; it is confirmed by the analyses reported here.

[1] Prell, W. L., Niitsuma, N., et al., 1991. *Proc. ODP, Sci. Results,* 117: College Station, TX (Ocean Drilling Program).

[2] Lamont-Doherty Geological Observatory of Columbia University, Palisades, NY 10964, U.S.A.

5. One of the authors (RDJ) participated in Leg 117, thus gaining access to cores and logs and obtaining familiarity with sometimes inadequately documented aspects of coring and logging quality and operations (e.g., the core swelling problem at Site 723).

6. Because of the major effort involved in obtaining sufficient XRF analyses for the core/log comparisons which are the primary focus of this project, it is desirable for the XRF analyses to be scientifically useful in themselves. Although not addressed in this paper, the paleoceanographic value of XRF analyses at these sites is substantial.

This evaluation of geochemical logs by comparison to XRF analyses is not the first such test. The precision and accuracy of the spectral gamma tool (K, Th, and U), gamma spectroscopy tool (Ca, Fe, Si, S, Ti, K, Gd, H, and Cl) and aluminum clay tool were established at the Conoco test well by comparison to neutron activation analyses of cores (Chapman et al., 1987). A recent symposium on geochemical well logging (Schlumberger, 1988) cites results of similar studies at several other petroleum-industry wells. Anderson et al. (in press) compare XRF and geochemical log data for four scientific drill holes, of which one is an ODP hole (Hole 504B, basalts and diabases). These studies indicate a remarkably high quality of geochemical logs. For example, assuming no XRF error and no depth error at the Conoco test well, Chapman et al. (1987) estimated the following precisions (expressed as weight percent standard deviations) for individual log-based elemental concentrations: 1% for Al, 2% for Ca, 0.5% for Fe, 0.25% for K, 1.5% for Si, 1.5% for S, and 0.1% for Ti.

However, these published analyses are probably not appropriate for ODP geochemical logs. ODP hole conditions are quite different from those in most industry wells; in particular, ODP sedimentary sequences are usually less lithified and consequently hole diameter is much less uniform. Because the ODP gamma spectroscopy tool (GST) has an outer diameter only slightly less than the drill pipe inner diameter, ODP has been unable to utilize the boron sleeve used in industry GST logging to reduce the dominance of chlorine counts over other elemental counts. Beginning with ODP Leg 126, a thin boron sleeve is being used now; its effect has not been quantitatively analyzed. The only published quantitative comparison of XRF and geochemical-log measurements at an ODP hole (504B) indicates only fair log accuracy (Anderson et al., 1989), though most ODP *Initial Reports* volumes report qualitative agreement of geochemical logs with visual core descriptions.

In this paper we report the results of 398 XRF analyses from ODP Sites 723, 728, and 731. We compare the XRF-based changes in elemental abundance as a function of depth with geochemical logs, to estimate the reliability of these geochemical logs. We also examine the inter-element patterns within the XRF data and evaluate the extent to which the geochemical logs exhibit these patterns.

METHODS

XRF

A total of 403 samples, each 10 cm^3, was taken from Holes 723B, 728B, and 731A. Except for the deepest 17 samples from Hole 731A and two dolomite samples from 723B, all sampling was focussed on short 5–30 m intervals with very good core recovery, with samples taken every 25 cm (Holes 723B and 728B) or 30 cm (Hole 731A). Departures from uniform sample spacing were permitted to avoid core disturbance and rare "gravy" between biscuits. However, sample locations were not chosen to preferentially sample specific lithologies; instead, this uniform very dense sampling was designed to obtain samples fully representative of the lithologic variations observed in cores, analogous to the continuous log measurements. Intervals were chosen for high resolution sampling primarily on the basis of core recovery and disturbance; a secondary criterion was avoidance of intervals that either visual core descriptions or geochemical logs suggested were homogeneous and relatively devoid of substantial geochemical variations.

At Site 723, core recovery was severely degraded by core expansion, attributed to high dissolved carbon dioxide. Based on the very high recoveries obtained in nearby sites at which core expansion was not a problem, we assume that each core began its trip to the surface with near-perfect recovery and that the lowest sediments in the core were forced through the core catcher and lost during core expansion, while tripping to the surface and before capping on board the ship. Prior to core splitting on board the ship, actively growing voids of a few centimeters to several meters in length were produced by the degassing. Our 25-cm post-cruise sampling of cores skipped across these voids, assuming original contiguity of the core pieces. Two sample depths are shown for each sample in Tables 1–3: an official "ODP depth" which is based on adding the current distance of the sample beneath the top of the core to the depth of the start of the cored interval, and a "true depth" which removes any core space occupied by voids. Only at Hole 723B did the ODP depth routinely differ from the "true" depth. In a subsequent section we will see one example of a core which appears to have lost recovery from the top of the core, rather than from the bottom.

Samples were prepared for analysis by freeze drying, disaggregation in a ball mill, and then pressing the powdered samples into pellets. Five samples were not subsequently analyzed; two were dolomites that resisted ball milling. Samples were not diluted prior to pressing into pellets; thus trace elements could be measured at concentrations of less than 100 parts per million (ppm). Chemical analyses were undertaken at the Oregon State University X-ray fluorescence facility, using a Phillips PW1600 X-ray Fluorescence Spectrometer with 25 fixed element detectors and 2 scanning LiF detectors to calculate X-ray background at each peak. Backgrounds were established from empirical relations between measured background points and background at each peak, based on a variety of blanks with different mean atomic numbers. Each batch of 19 samples included a monitor standard. After backgrounds were stripped for each sample, stripped data were normalized to the monitor standard to eliminate minor machine drift. Concentrations were calculated using the XRF11 G program (Chriss software), calibrated with over 100 geological standards and mixtures amongst standards. Precision based upon multiple measurements of an in-house standard was approximately 3% for Na and 1% or better for the other major elements.

Based on inter-batch comparison of the monitor standard, almost half of the trace element analyses are unreliable. Unreliable results, encompassing the deepest samples from Site 728 and all samples from Site 731, occurred only after an electrical cable replacement. Financial constraints precluded the desirable total recalibration of the system following this change. Samples with unreliable trace element abundances are indicated by an asterisk in Tables 2 and 3. Inter-batch comparison of the monitor standard demonstrated that major element analyses were not affected by this change.

Porosities of the samples were about 60% at Sites 723 and 728 and 45%–70% at Site 731 (Prell, Niitsuma, et al., 1989). Thus correction was warranted for pore-water sea salt, left in each sample by the drying process. The salt percentage in each sample was calculated from the chlorine concentration, using the average measured chlorinity (Prell, Niitsuma, et al., 1989) of interstitial waters at Sites 728 and 731 and the broad chlorinity-vs.-depth trend of Site 723. Elemental concentrations were

then corrected for dilution by the salt mass. Further, Na, Ca, Mg, and K sea-salt contributions were calculated and subtracted out, utilizing the shipboard measurements of concentrations of these elements in interstitial waters. Corrected XRF results for the three sites are listed in Tables 1–3. Blank spaces in the Na column indicate the rare cases in which the sea-salt correction produced a negative Na concentration. Salt percentages are also shown, to permit backtracking to raw data.

Data were not corrected for calcite dilution in each sample, but a normative calcite correction can be made:

$$CaCO_3\% = K_{cc} \times Ca_{tot} - K_{cc} \times Ca_n/(1 - (Ca_n \times K_{cc}/100)),$$

where $K_{cc} = 2.5$ is the conversion factor from Ca% to calcite%, Ca_n is the calcium percentage of the noncalcite fraction (typically 0.7%), and Ca_{tot} is the total Ca% measured by XRF.

Because the focus of this paper is on geochemical log comparison with cores, only the major elements from Tables 1–3 will be discussed in subsequent sections. Geochemical logs do yield concentrations for the trace elements Th, U, and Gd. However, Gd cannot be determined by XRF, and the Th and U concentrations shown in Tables 1–3 are clearly near the noise level of the instrument.

Logs

The geochemical string consists of three logging tools. The natural gamma tool (NGT) measures the spectrum of natural gamma rays emitted by the formation; inversion of the spectrum yields concentrations of K (%), Th (ppm), and U (ppm) (Lock and Hoyer, 1971; Serra et al., 1980). The aluminum clay tool (ACT) uses two NGT's and an intermediate californium source of neutrons; the difference between NGT spectra for irradiated and unirradiated formation is inverted for aluminum concentration (%) of the formation (Scott and Smith, 1973). The gamma spectroscopy tool (GST) irradiates the formation with a neutron generator and measures the spectrum of immediately induced gamma rays (Hertzog, 1979). This recorded spectrum is inverted in real time for counts of Cl, H, Ca, Si, Fe, and S. In post-cruise reprocessing, a significant improvement in inversion quality is achieved by inverting for Ti, K, and Gd in addition to the six elements above. That gadolinium, present in the formation in ppm, could affect an inversion for calcium, present in percent, is initially surprising but follows from the immense neutron capture cross section of Gd, compared to that of Ca. Potassium determined from the GST is substantially lower in accuracy than that from the NGT; in practice, the NGT potassium is usually used to determine the error in GST K, and the residual GST K is repartitioned to the other GST elements. If all three geochemical tools are run and a log of photoelectric effect is also obtained, Schlumberger software also solves for Mg + Na, by attributing the difference between predicted and observed photoelectric effect to Mg + Na (Hertzog et al., 1987). With all of the major elements thereby determined, the proprietary algorithm solves for major-element oxide dry-weight percentages.

On ODP Leg 117, the complete geochemical log suite plus photoelectric effect log was obtained only at Site 723, for the openhole interval 92–424 mbsf. At Site 728 the NGT and GST were run over the interval 0–342 mbsf; of this interval, the top 56 m were logged through pipe and the remainder were openhole logs. At Site 731 the NGT and GST were run over the interval 0–979 mbsf; of this interval, the top 65 m were logged through pipe and the remainder were openhole logs. In this paper we consider only openhole logs, which are more reliable than those obtained through pipe.

The *Initial Reports* for Leg 117 show geochemical data for Site 723 as weight-percent oxides. GST data for Sites 728 and 731 were shown as yields determined by postcruise 9-element inversion, because insufficient tools were run for determination of weight-percent oxides. These are two of the most common processing outputs shown in *Initial Reports* volumes, though sometimes only the 6-element inversion results are shown due to processing delays. However, we use a different geochemical log processing in this paper. We consider the oxide determination published for Site 723 to be unreliable for two reasons. First, the conversion from elemental yields to oxides assumed cation/oxygen ratios appropriate for igneous rocks, not for sediments. Second, the photoelectric effect determination of Mg + Na failed, causing the algorithm to use a default Mg estimation technique. However, XRD results for the site (Cremer et al., this volume) indicate only minor dolomite; the Mg is in clay minerals. As we shall see subsequently, Mg is inversely correlated with Ca, not positively correlated as assumed by our previous oxide inversion (Prell, Niitsuma, et al., 1989).

Our geochemical log processing begins with the 9-element GST inversion. We then repartition the GST-determined Cl and K. The need for Cl repartitioning is demonstrated by the high and predictable correlation between Cl and other elemental yields. For example, we have observed that the correlation coefficient between Ca and Cl yields is minus 0.3–0.5 in a wide variety of ODP lithologies. More compelling is our observation that the slopes of regression lines between Cl yields and Ca, Fe, Si, Ti, K, and Gd yields at Sites 723, 728, and 731 are extremely similar to the proprietary Schlumberger repartitioning coefficients for Cl. Thus we may assume that nearly all of the small-scale Cl-yield character is a partitioning problem, and repartition it to the other elements. The broad-scale character, associated with compaction-induced porosity reduction with depth and—at Site 723—with gradual chlorinity changes, was estimated as follows: (1) Site 728: a first-degree regression of Cl on depth; (2) Site 723: a second-degree regression of Cl on depth; (3) Site 731: a linear trend for the interval 65–494 mbsf and a constant Cl baseline beneath 494 mbsf.

We used the Schlumberger repartitioning coefficients rather than our regression estimates of these coefficients, because a correlation of porosity with mineralogy (e.g., higher porosity clays than carbonates) could have a slight effect on our regression estimates. However, we shall see subsequently (Figs. 11–13) that XRF data exhibit little to no correlation of porosity with mineralogy.

The need for K repartitioning is indicated by three observations. First, a substantial portion of the K yields are negative (e.g., Fig. 1); this result can only be caused by inversion error. Second, K yields are much higher for through-pipe logs than openhole logs. Pipe is actually lower in K than is the formation; the observed difference results from the fact that lower Cl counts through-pipe cause higher apparent K counts. Third, the correlation between NGT K and GST K is near zero; this observation indicates that there is virtually no information in the GST K yield concerning actual formation variations in K. An extreme example of this conclusion is illustrated in Figure 1, which shows K yields across the transition from relatively pure carbonates to terrigenous turbidites at Site 731. Based on our XRF measurements, K increases from an average of 0.8% to 2.6% across this transition, but no change is detectable on the GST log of K yield. We therefore repartitioned all of the K yield to the other GST elements. We did not follow the normal Schlumberger approach of repartitioning only the difference between GST K yield and predicted K yield from the NGT. To do so would be to assume that NGT K is perfectly accurate (an assumption whose validity this study tests) and would cause a ripple effect of NGT K on the GST yields of other elements, contrary to our preference for independent tests of NGT and GST accuracy.

Table 1. Hole 723B XRF data.

Core no.	Sec no.	Sec depth (cm)	ODP depth (mbsf)	True depth (mbsf)	Na (%)	Mg (%)	Al (%)	Si (%)	P (%)	S (%)	K (%)	Ca (%)	Ti (%)	Cr (%)	Mn (%)	Fe (%)	Co (ppm)	Ni (ppm)	Cu (ppm)	Zn (ppm)	Rb (ppm)	Sr (ppm)	Ba (ppm)	La (ppm)	Pb (ppm)	Th (ppm)	U (ppm)	Salt (%)
11	2	38	93.08	92.74	0.41	3.25	2.96	12.6	0.078	0.644	1.011	18.9	0.281	0.0223	0.0638	2.05	14	36	222	55	42	679	321	18	13	1	3	1.88
11	2	63	93.33	92.99	0.5	3.23	3.05	13.2	0.071	0.571	0.99	19	0.29	0.0251	0.0636	2.04	14	25	222	33	39	667	307	18	13	0	3	1.69
11	2	104	93.74	93.24	0.44	3.25	3.07	13.2	0.079	0.672	1.014	18.4	0.294	0.0267	0.0639	2.16	16	52	222	43	46	658	139	26	13	0	3	2.07
11	2	133	94.03	93.49	0.45	3.15	3.03	13	0.078	0.61	0.996	19	0.291	0.0242	0.0638	2.05	13	29	222	32	44	694	312	29	13	2	3	2
11	3	12	94.32	93.73	0.4	3.11	2.94	12.6	0.085	0.561	0.968	19.7	0.278	0.0218	0.0637	2.06	15	35	223	48	43	742	338	19	13	0	3	1.86
11	3	38	94.58	93.99	0.39	2.89	2.92	12.6	0.085	0.625	0.972	19.2	0.28	0.0255	0.0639	2.1	16	52	224	67	46	724	314	19	13	0	3	2.1
11	3	61	94.81	94.22	0.39	2.77	2.82	11.9	0.092	0.633	0.934	19.8	0.269	0.0238	0.0638	2.09	17	46	225	48	43	778	328	36	13	0	3	1.88
11	3	132	95.52	94.68	0.26	2.68	2.24	9.2	0.139	0.736	0.728	23.6	0.208	0.0177	0.0642	1.46	14	48	231	80	45	980	29	38	13	3	3	2.58
11	4	22	95.92	95.08	0.26	2.65	2.27	9.4	0.143	0.731	0.715	23.3	0.209	0.0192	0.0642	1.5	13	56	231	89	42	971	92	27	13	0	3	2.52
11	4	45	96.15	95.31	0.32	2.8	2.33	9.7	0.135	0.691	0.714	23.6	0.215	0.0196	0.0641	1.46	11	52	231	90	39	842	54	27	13	0	3	2.44
11	4	70	96.4	95.56	0.38	2.96	2.5	10.5	0.133	0.642	0.772	22.6	0.238	0.0223	0.0639	1.59	7	44	228	71	42	861	145	27	13	3	3	2.07
11	4	109	96.79	95.81	0.4	3.07	2.6	11.1	0.139	0.603	0.817	21.6	0.25	0.0262	0.0639	1.7	5	43	227	55	40	790	168	20	13	0	3	2.04
11	4	133	97.03	96.05	0.39	3.19	2.62	11.1	0.143	0.575	0.83	21.6	0.249	0.0219	0.0637	1.7	4	42	226	59	40	789	271	20	13	0	3	1.86
11	5	10	97.3	96.02	0.41	3.97	2.68	11.2	0.122	0.534	0.835	21	0.249	0.0202	0.0637	1.72	5	31	224	42	43	564	330	25	13	3	3	1.75
11	5	33	97.53	96.25	0.47	4.24	2.98	12.4	0.085	0.44	0.928	19.9	0.275	0.0231	0.0636	1.86	6	25	222	69	37	669	273	23	13	0	3	1.7
11	5	128	98.48	96.85	0.47	3.81	3	13.1	0.074	0.475	0.959	19.1	0.288	0.0281	0.0636	1.96	7	19	221	36	37	595	335	21	13	1	3	1.67
11	6	1	98.71	97.08	0.55	3.83	3.05	13.4	0.072	0.455	0.967	19	0.297	0.0308	0.0635	1.96	8	22	220	34	39	595	322	25	13	0	3	1.45
11	6	48	99.18	97.33	0.44	3.73	2.84	12.3	0.08	0.588	0.919	19.1	0.28	0.0289	0.0638	1.93	9	40	221	35	43	624	260	29	13	3	3	1.87
11	6	73	99.43	97.58	0.4	3.51	2.84	12.3	0.079	0.708	0.934	18.6	0.277	0.0277	0.0637	1.99	7	49	221	36	45	578	347	25	13	1	3	1.73
11	6	98	99.68	97.83	0.41	3.33	2.85	12.5	0.085	0.752	0.942	18.3	0.291	0.0291	0.0637	2.09	8	57	221	44	44	570	275	20	13	1	3	1.72
11	6	123	99.93	98.08	0.42	3.02	2.88	12.6	0.075	0.778	0.947	18.7	0.296	0.03	0.0638	2.12	7	58	222	38	43	609	332	19	13	0	3	1.95
11	6	148	100.18	98.33	0.38	3.1	2.82	12.4	0.081	0.662	0.931	18.8	0.286	0.0256	0.0638	2.05	7	53	222	41	43	616	373	23	13	0	3	1.96
11	7	23	100.43	98.43	0.41	3.09	2.94	12.9	0.076	0.693	0.974	18.5	0.3	0.0262	0.0638	2.14	7	64	222	39	45	599	248	23	13	0	3	1.94
11	7	41	100.61	98.61																								
11	CC	13	100.65	98.65	0.5	3.44	3.09	13.5	0.075	0.502	0.984	18.9	0.306	0.0266	0.0635	2.09	8	44	220	36	39	597	330	23	13	0	3	1.51
11	CC	38	100.9	98.9	0.42	3.12	2.88	12.5	0.091	0.641	0.932	19.1	0.283	0.0252	0.0636	2	7	42	222	39	46	648	373	19	13	2	3	1.63
12	1	23	100.93	100.93	0.27	2.1	2.48	10	0.076	0.565	0.826	22.2	0.237	0.016	0.0638	1.81	7	48	229	53	41	1465	262	19	14	0	3	1.94
12	1	51	101.21	101.16	0.2	2.13	2.43	9.8	0.072	0.597	0.814	22.8	0.238	0.0152	0.0641	1.8	6	58	231	48	42	1415	159	38	14	0	3	2.36
12	1	74	101.44	101.39	0.39	2.5	2.77	11.8	0.082	0.52	0.895	20.3	0.274	0.0238	0.0637	2.05	7	51	226	43	36	796	341	21	13	0	3	1.78
12	1	101	101.71	101.64	0.36	2.51	2.77	11.7	0.076	0.536	0.909	20.6	0.279	0.0214	0.0637	2.07	8	51	226	49	40	1034	289	21	13	0	3	1.72
12	1	124	101.94	101.87	0.35	2.47	2.75	11.5	0.069	0.53	0.914	20.6	0.27	0.0193	0.0637	2.08	7	48	227	43	39	1102	364	22	13	0	3	1.81
12	1	148	102.18	102.11	0.31	2.5	2.79	11.5	0.061	0.455	0.929	21	0.26	0.0172	0.0638	2.01	9	47	227	45	44	1139	327	22	13	1	3	1.93
12	2	23	102.43	102.36	0.34	2.41	2.8	11.6	0.056	0.446	0.92	21.3	0.267	0.017	0.0638	1.99	7	35	227	51	43	1123	332	37	13	2	3	1.9
12	2	51	102.71	102.63	0.32	2.58	2.83	11.6	0.061	0.505	0.941	20.8	0.265	0.0169	0.0638	2.05	9	52	226	58	45	1057	342	37	13	3	3	1.9
12	2	73	102.93	102.85	0.3	2.25	2.64	10.8	0.052	0.485	0.884	21.8	0.25	0.0154	0.0636	1.92	7	44	228	49	39	1317	309	26	13	0	3	1.7
23	1	25	207.15	207.15	0.05	1.63	1.5	6	0.152	0.736	0.473	27.6	0.132	0.0096	0.0642	1.04	3	45	239	82	37	1370	318	22	14	2	3	2.53
23	1	50	207.4	207.4	0.04	1.74	1.7	6.8	0.17	0.716	0.562	26	0.153	0.0099	0.0641	1.25	1	47	237	63	43	1307	366	20	14	0	3	2.4
23	2	31	208.71	207.63	0.12	1.8	1.72	7.1	0.203	0.709	0.555	26	0.164	0.0107	0.064	1.31	4	49	236	73	43	1304	325	23	14	0	3	2.3
23	2	58	208.98	207.9	0.09	1.81	1.73	7.3	0.229	0.747	0.577	25.3	0.17	0.0119	0.0641	1.36	3	56	235	63	47	1289	349	22	14	0	3	2.33
23	2	83	209.23	208.15	0.13	2.12	1.87	9	0.232	0.939	0.602	22.9	0.188	0.0134	0.0642	1.53	5	75	232	78	48	1176	262	21	14	0	3	2.55
23	2	106	209.46	208.38	0.1	2	1.64	8.1	0.23	0.802	0.515	25	0.167	0.0108	0.0641	1.31	3	44	235	53	42	1270	292	23	14	0	3	2.44
23	2	131	209.71	208.63	0.15	2.32	1.85	11.1	0.199	0.919	0.588	21.5	0.19	0.0172	0.0643	1.54	4	74	228	59	43	1002	146	21	13	0	3	2.65
23	3	6	209.96	208.88	0.14	2.01	1.81	8.1	0.181	0.85	0.59	24	0.186	0.0154	0.0642	1.51	5	63	234	59	41	1168	265	21	14	0	3	2.48
23	3	31	210.21	209.13	0.14	1.99	2	8.3	0.105	0.704	0.653	23.8	0.201	0.0153	0.0639	1.68	3	50	233	46	40	1241	225	25	14	0	3	2.16
23	3	56	210.46	209.38	0.13	1.74	1.85	7.7	0.114	0.736	0.602	24.6	0.189	0.0155	0.064	1.56	3	59	235	50	40	1263	253	21	14	0	3	2.29
23	3	81	210.71	209.63	0.19	1.86	2	8.1	0.105	0.713	0.653	24.3	0.198	0.0156	0.0638	1.59	5	60	233	53	41	1247	289	19	14	0	3	1.9
23	3	106	210.96	209.88	0.13	1.85	1.87	7.7	0.104	0.689	0.614	25	0.18	0.015	0.0639	1.46	4	48	235	59	38	1270	227	23	14	0	3	2.07
23	3	131	211.21	210.13	0.17	2.01	2.15	8.6	0.1	0.693	0.706	24.1	0.202	0.0146	0.064	1.62	4	56	233	57	39	1187	225	20	14	0	3	2.24
23	4	6	211.46	210.36	0.17	2.04	2.19	8.6	0.097	0.68	0.731	23.6	0.197	0.0133	0.0639	1.63	4	50	232	63	41	1163	224	19	14	0	3	2.14
23	4	39	211.79	210.6	0.22	2.24	2.27	9	0.101	0.695	0.739	23.4	0.205	0.0144	0.0639	1.63	5	56	232	56	43	1150	198	21	14	0	3	2.04
23	4	64	212.04	210.85	0.22	2.34	2.2	8.6	0.11	0.704	0.723	23.7	0.195	0.0137	0.0639	1.59	5	57	232	60	39	1150	109	24	14	0	3	2.04
23	4	89	212.29	211.1	0.22	2.36	2.24	8.8	0.123	0.72	0.723	23.1	0.203	0.0155	0.064	1.64	5	56	231	55	42	1128	299	20	14	0	3	2.21
23	4	123	212.63	211.38	0.22	2.14	2.01	7.9	0.159	0.818	0.644	24.3	0.192	0.0171	0.0641	1.5	3	54	234	54	45	1172	371	21	14	0	3	2.46
23	5	14	213.04	211.73	0.31	2.58	2.59	10.3	0.269	0.847	0.833	20.8	0.245	0.0185	0.064	2.06	7	86	228	59	51	947	28	37	13	0	3	2.21
23	5	35	213.25	211.94	0.24	2.22	2.54	10.5	0.169	0.979	0.811	20.1	0.251	0.0252	0.0643	2.12	7	94	228	93	52	910	28	22	14	1	3	2.75
23	5	92	213.82	212.23	0.31	2.04	2.43	10.2	0.164	0.969	0.786	20.8	0.253	0.0243	0.0639	2.07	8	110	229	95	50	840	29	19	14	0	3	2.06
23	5	117	214.07	212.48	0.18	2.04	2.12	8.9	0.144	0.852	0.692	22.4	0.215	0.0195	0.064	1.84	6	89	231	73	48	1099	121	21	14	0	3	2.3
23	5	142	214.32	212.73	0.17	2.07	2.12	8.7	0.124	0.867	0.691	22.6	0.199	0.0169	0.064	1.77	7	93	231	84	45	1102	92	23	14	0	3	2.26
23	6	17	214.57	212.98	0.13	1.96	2.03	8.3	0.121	0.907	0.672	23.3	0.19	0.0148	0.0641	1.67	5	83	233	76	52	1181	288	20	14	0	3	2.38
23	6	39	214.79	213.2	0.09	1.72	1.69	6.8	0.124	0.894	0.56	26	0.148	0.0113	0.0641	1.29	4	71	237	81	48	1339	260	22	14	0	3	2.46
23	6	64	215.04	213.45	0.06	1.67	1.55	6.1	0.133	0.932	0.515	26.7	0.14	0.0114	0.0642	1.17	3	74	238	77	51	1372	382	22	14	0	3	2.53
23	6	89	215.29	213.7	0.11	1.7	1.65	6.7	0.144	0.874	0.551	25.8	0.155	0.0127	0.064	1.29	5	73	236	86	49	1284	204	26	14	0	3	2.26
23	6	110	215.5	213.91	0.12	1.79	1.83	7.5	0.133	0.801	0.612	25.1	0.171	0.0129	0.064	1.43	4	64	235	76	46	1242	293	28	14	0	3	2.32
23	7	15	216.05	214.22	0.19	1.9	1.9	8.2	0.149	0.737	0.627	24	0.192	0.015	0.0639	1.55	3	45	233	54	44	1123	161	20	14	0	3	2.14
23	7	41	216.31	216.31																								
23	CC	21	216.43	214.6	0.2	2.18	1.93	8.3	0.142	0.735	0.625	24.1	0.188	0.0159	0.0641	1.54	4	56	234	56	40	1161	29	23	14	0	3	2.42
24	1	25	216.75	216.75	0.26	2.22	2.43	10	0.144	0.753	0.801	21.6	0.239	0.0186	0.0639	1.97	7	87	229	62	48	993	29	27	14	0	3	2.17
24	1	50	217	217	0.24	2.23	2.42	9.8	0.156	0.823	0.81	21.3	0.235	0.0185	0.064	1.97	8	101	229	66	52	882	29	20	14	0	3	2.18
24	1	74	217.24	217.24	0.31	2.36	2.8	11.4	0.17	0.866	0.92	19.4	0.276	0.0232	0.0639	2.29	9	106	226	81	53	886	28	21	13	0	3	2.06
24	1	115	217.65	217.5	0.3	2.12	2.78	12.5	0.204	1.09	0.937	17.9	0.284	0.0223	0.0642	2.39	9	159	225	97	58	753	28	22	13	0	3	2.49
24	1	137	217.87	217.72	0.36	2.49	3.03	12.5	0.231	0.683	0.988	19.1	0.28	0.0231	0.0638	2.46	10	89	225	60	50	830	28	21	13	0	3	1.96
24	2	15	218.15	218	0.28	1.98	2.58	10.5	0.121	0.892	0.857	20.5	0.255	0.0207	0.064	2.22	9	109	229	83	49	931	78	20	14	0	3	2.25
24	2	37.5	218.375	218.23	0.2	1.64	2.18	9.1	0.145	0.973	0.727	22.2	0.223	0.0191	0.0641	1.92	6	105	232	79	47	1071	172	20	14	0	3	2.41
24	2	63	218.63	218.48		0.94	1.46	23.8	0.088	1.076	0.443	12.7	0.163	0.0133	0.0654	1.51	8	90	211	119	54	733	242	18	14	13	3	4.35

24	2	90	218.9	218.75	0.36	2.34	3.06	12.5	0.144	0.657	0.997	19.3	0.278	0.0218	0.0637	2.4	7	77	225	49	51	885	28	19	13	2	3	1.85
24	2	113	219.13	218.98	0.2	1.82	2.41	9.9	0.148	0.866	0.786	21.6	0.233	0.0195	0.0639	1.99	7	79	230	73	51	1044	257	18	14	0	3	2.11
24	3	11	219.61	219.23	0.23	1.86	2.52	10.5	0.139	0.944	0.81	21.1	0.236	0.0184	0.0641	2.06	7	86	229	70	58	893	29	18	14	2	3	2.39
24	3	51	220.01	219.5	0.14	1.72	2.15	9	0.168	1.015	0.713	22.9	0.192	0.0152	0.064	1.69	5	92	232	92	56	1146	278	23	14	0	3	2.32
24	3	90	220.4	219.74	0.09	1.52	1.84	7.7	0.132	1.008	0.613	24.8	0.155	0.0111	0.0641	1.36	3	76	235	84	60	1292	272	28	14	0	3	2.46
24	3	114	220.64	219.98	0.03	1.28	1.37	5.7	0.155	0.945	0.443	27.9	0.114	0.008	0.0644	0.97	0	59	241	81	56	1457	347	32	14	1	3	2.8
24	3	148	220.98	220.23	0.06	1.5	1.67	7.4	0.263	1.012	0.56	25.2	0.15	0.0118	0.0643	1.29	0	75	235	80	59	1310	56	23	14	0	3	2.74
24	4	33	221.33	220.5	0.1	1.63	1.71	8.2	0.263	0.984	0.558	24.5	0.161	0.0135	0.0643	1.37	4	80	234	83	58	1258	189	21	14	0	3	2.71
24	4	61	221.61	220.78	0.06	1.55	1.68	7.9	0.267	1.026	0.549	24.4	0.158	0.0121	0.0643	1.39	3	97	234	72	62	1263	68	24	14	0	3	2.77
24	4	83	221.83	221	0.12	1.39	1.74	9.4	0.188	1.049	0.556	23.3	0.171	0.015	0.0644	1.49	4	91	233	79	55	1206	226	27	14	0	3	2.89
24	4	108	222.08	221.25	0.13	1.18	2.01	15.7	0.245	1.005	0.777	18	0.183	0.0157	0.0647	1.6	5	87	222	86	61	949	28	21	13	2	3	3.3
24	4	133	222.33	221.5	0.1	1.5	2.12	14.2	0.159	1.173	0.695	18.4	0.227	0.0209	0.0647	1.91	7	118	225	113	61	884	65	19	13	1	3	3.37
24	5	8	222.58	221.75	0.26	1.89	2.51	13.3	0.233	0.885	0.795	19.5	0.25	0.0213	0.0642	2.18	8	103	226	87	60	922	28	21	13	2	3	2.59
24	5	33	222.83	222	0.28	2.04	2.64	12.8	0.112	0.787	0.843	19.9	0.247	0.019	0.0639	2.12	9	99	226	88	54	863	118	20	13	0	3	2.15
24	5	63	223.13	222.22	0.26	2.04	2.47	11.6	0.098	0.763	0.81	21	0.227	0.019	0.064	1.89	7	86	227	93	59	979	272	21	13	3	3	2.25
24	6	5	224.05	222.47	0.18	2.09	2.03	9.7	0.089	0.778	0.667	23.2	0.182	0.0137	0.0641	1.55	5	71	231	113	55	1150	316	25	14	0	3	2.34
24	6	30	224.3	222.72	0.34	2.68	2.74	11.4	0.085	0.622	0.9	20.9	0.242	0.0161	0.0639	2.01	7	74	227	80	55	847	28	21	13	0	3	2.15
24	6	105	225.05	222.98	0.42	3.28	3.27	13.2	0.076	0.522	1.06	18.8	0.276	0.018	0.0637	2.34	9	78	222	71	53	789	28	20	13	0	3	1.82
24	6	129	225.29	223.22	0.41	3.84	3.34	13.3	0.072	0.485	1.081	18.3	0.282	0.017	0.0634	2.38	10	74	220	58	48	740	149	23	13	0	3	1.37
24	7	5	225.55	223.48	0.43	4.4	3.42	13.5	0.071	0.438	1.099	17.5	0.284	0.0183	0.0637	2.42	10	69	219	59	52	681	219	19	13	1	3	1.77
24	7	30	225.8	223.73	0.46	4.29	3.41	13.6	0.07	0.462	1.085	17.8	0.288	0.02	0.0634	2.39	9	61	219	46	49	704	258	19	13	1	3	1.29
24	CC	11	226.04	223.97	0.39	3.71	3.22	12.7	0.078	0.531	1.044	18.4	0.278	0.0191	0.0637	2.38	10	85	222	83	50	775	409	36	13	1	3	1.84
24	CC	36	226.29	224.22	0.39	3.69	3.19	12.6	0.083	0.594	1.023	18.4	0.279	0.02	0.0636	2.37	10	88	222	59	54	684	321	36	13	1	3	1.65
24	CC	61	226.54	224.47	0.36	2.99	3.09	12.3	0.086	0.661	1.007	18.7	0.278	0.0205	0.0639	2.37	10	84	224	89	52	815	28	36	13	2	3	2.11
24	CC	86	226.79	224.72	0.24	2.3	2.72	11	0.094	0.856	0.897	19.4	0.255	0.0217	0.064	2.29	9	99	227	144	55	930	40	30	14	2	3	2.23
25	1	25	226.45	226.45	0.11	1.54	1.74	8.5	0.261	1.221	0.565	22.5	0.176	0.0167	0.0644	1.44	4	108	232	91	72	1102	148	31	14	3	3	2.85
25	1	50	226.7	226.7	0.1	1.67	1.89	9.9	0.184	1.171	0.618	21.6	0.191	0.018	0.0644	1.61	7	117	230	108	68	1061	29	27	14	2	3	2.78
25	1	75	226.95	226.95	0.14	1.84	2.11	10.7	0.117	1.002	0.698	20.8	0.212	0.016	0.0643	1.84	6	103	229	98	62	1041	66	20	14	5	3	2.66
25	1	138	227.58	227.2	0.13	1.87	1.98	8.9	0.101	0.843	0.645	23.1	0.19	0.0145	0.0642	1.64	6	66	233	77	53	1140	29	22	14	3	3	2.51
25	2	13	227.83	227.45	0.11	2	1.98	8.5	0.106	0.817	0.654	23.6	0.185	0.0143	0.0641	1.55	4	74	233	69	56	1168	93	24	14	1	3	2.43
25	2	47	228.17	227.71	0.1	1.94	1.95	8.2	0.111	0.877	0.655	23.4	0.174	0.0148	0.0641	1.53	6	78	232	86	62	1175	29	23	14	5	3	2.33
25	2	70	228.4	228.4	0.06	1.87	1.6	6.5	0.098	0.944	0.532	25.7	0.136	0.0104	0.0641	1.2	6	63	236	82	63	1360	43	22	14	3	3	2.43
25	2	134	229.04	228.23	0.15	2.13	2.02	8.4	0.114	0.791	0.686	23.7	0.18	0.0128	0.0641	1.5	4	63	233	70	51	1188	119	31	14	1	3	2.42
25	3	9	229.29	228.48	0.28	2.36	2.44	10.2	0.132	0.693	0.806	22	0.216	0.0142	0.0641	1.79	6	58	230	77	58	1067	29	37	13	1	3	2.42
25	3	34	229.54	228.73	0.33	2.51	2.82	11.4	0.106	0.633	0.93	20.7	0.244	0.0166	0.0638	1.99	8	66	227	63	55	933	28	23	13	3	3	2.02
25	3	59	229.79	228.98	0.33	2.44	2.87	11.5	0.106	0.627	0.948	20.6	0.248	0.017	0.0638	2.01	7	57	226	65	50	827	127	20	13	0	3	1.98
25	3	91	230.11	229.22	0.3	2.27	2.68	10.8	0.114	0.669	0.879	21.4	0.239	0.0182	0.0639	1.87	6	58	228	63	51	975	115	19	13	0	3	2.14
25	3	114	230.34	229.45	0.23	2.01	2.28	9.2	0.121	0.795	0.737	23.2	0.213	0.0165	0.064	1.61	7	49	231	105	60	1092	122	20	14	4	3	2.27
25	3	138	230.58	229.69	0.22	2.03	2.27	9.1	0.133	0.856	0.74	22.9	0.216	0.0174	0.0641	1.66	5	60	232	60	60	1064	109	25	14	0	3	2.38
25	4	25	230.95	229.95	0.26	2.06	2.31	9.5	0.143	0.838	0.731	22.6	0.227	0.0192	0.0642	1.68	7	56	231	77	55	1049	54	38	14	0	3	2.52
25	4	50	231.2	230.2	0.29	2.17	2.47	10	0.151	0.917	0.799	21.3	0.233	0.0209	0.0641	1.84	8	81	229	80	61	981	78	23	14	2	3	2.43
25	4	81	231.51	230.44	0.27	2.14	2.45	9.9	0.151	0.854	0.806	21.4	0.234	0.0197	0.064	1.84	6	59	229	72	69	875	41	19	14	0	3	2.32
25	4	113	231.83	230.7	0.26	2.03	2.44	9.9	0.15	0.999	0.805	21.2	0.228	0.0213	0.0639	1.85	8	81	229	92	70	871	170	21	14	2	3	2.16
25	4	138	232.08	230.95	0.23	1.96	2.35	9.7	0.159	0.923	0.776	21.7	0.228	0.0199	0.0641	1.79	9	89	229	104	71	1004	103	23	14	2	3	2.36
25	5	72	232.92	231.2	0.22	1.88	2.19	9	0.163	0.984	0.719	22.3	0.209	0.0191	0.0641	1.65	7	72	231	76	68	1045	105	19	14	0	3	2.46
25	5	97	233.17	231.45	0.25	1.99	2.32	9.5	0.159	0.939	0.759	21.9	0.218	0.0193	0.064	1.72	7	76	229	123	65	904	41	21	14	3	3	2.28
25	5	119	233.39	231.67	0.22	1.99	2.25	9.3	0.18	1.018	0.741	21.8	0.218	0.0198	0.0641	1.72	7	86	229	105	80	1024	29	23	14	3	3	2.36
25	5	147	233.67	231.95	0.2	1.92	2.12	8.7	0.179	0.953	0.7	22.9	0.205	0.0173	0.0642	1.61	6	70	232	83	73	1087	54	21	14	0	3	2.51
25	6	22	233.92	232.2	0.26	2.07	2.31	9.6	0.193	1.005	0.754	21.3	0.223	0.0191	0.0641	1.77	6	83	228	86	82	976	29	22	14	3	3	2.37
25	6	47	234.17	232.45	0.26	2.17	2.41	10	0.159	0.906	0.8	20.9	0.227	0.0205	0.0639	1.85	7	88	228	93	78	949	29	22	14	0	3	2.14
25	6	100	234.7	232.53																								
25	6	118	234.88	232.71	0.31	2.36	2.67	11.1	0.155	0.897	0.887	19.7	0.256	0.0221	0.0639	2.03	10	92	226	99	79	879	40	26	14	2	3	2.07
25	7	11	235.31	232.95	0.36	2.4	2.73	11.4	0.147	0.993	0.897	19.4	0.256	0.0211	0.064	2.07	8	90	225	92	76	843	28	26	13	0	3	2.21
25	7	36	235.56	233.2	0.37	2.71	2.97	12.2	0.167	0.953	0.969	18.1	0.276	0.0244	0.0641	2.24	10	106	223	108	86	776	164	26	13	3	3	2.37
25	CC	21	235.75	233.43	0.36	2.56	2.72	11.1	0.151	0.858	0.897	19.6	0.255	0.0222	0.0638	2.04	8	88	225	94	78	845	101	25	13	3	3	1.89
25	CC	46	236	233.68	0.32	2.48	2.73	11	0.142	0.869	0.893	20	0.257	0.021	0.0639	2.02	7	67	226	103	65	862	126	26	13	2	3	2.11
27	CC	20	247.2	246.98																								
33	CC	26	317.09	316.16																								
41	1	25	381.25	381.25	0.25	1.6	2.45	10.4	0.134	1.021	0.801	21	0.243	0.0207	0.0641	1.94	9	85	230	101	51	1075	29	30	14	1	3	2.4
41	1	50	381.5	381.5	0.2	1.54	2.33	9.5	0.133	1.062	0.765	22	0.219	0.0166	0.064	1.85	7	73	231	84	50	1139	54	25	14	0	3	2.27
41	1	81	381.81	381.75	0.16	1.35	1.96	7.7	0.127	1.015	0.654	24.7	0.175	0.0125	0.064	1.5	6	61	235	85	47	1313	163	27	14	2	3	2.29
41	1	106	382.06	382	0.04	1.04	1.33	5	0.123	0.86	0.434	29.2	0.112	0.0081	0.0639	0.93	1	25	242	55	40	1590	662	26	14	0	3	2.13
41	1	129	382.29	382.23	0.03	0.93	1.07	3.8	0.105	0.778	0.319	31.5	0.086	0.0061	0.0641	0.65	0	14	246	52	35	1708	242	23	14	0	3	2.39
41	2	6	382.56	382.49	0.05	1.05	1.25	4.6	0.119	0.82	0.393	30.1	0.103	0.008	0.064	0.81	3	16	244	52	42	1619	72	24	14	2	3	2.3
41	2	28	382.78	382.71	0.14	1.22	1.66	6.7	0.135	0.933	0.563	26.3	0.148	0.0116	0.0639	1.24	4	42	237	55	43	1343	392	22	14	0	3	2.14
41	2	59	383.09	383.02	0.48	2.17	3.9	22.9	0.34	1.561	1.289	6.6	0.406	0.0361	0.0645	3.35	20	198	205	150	86	361	685	18	12	7	3	3.08
41	2	99	383.49	383.25	0.38	1.9	3.34	18.8	0.164	1.381	1.111	11.5	0.342	0.0314	0.0643	3.03	15	154	214	86	76	517	94	24	13	3	3	2.68
41	3	3	384.03	383.55	0.56	2.25	4.28	19.9	0.196	1.665	1.406	8.2	0.423	0.0378	0.0642	3.63	20	213	209	113	86	425	523	18	13	7	3	2.61
41	3	47	384.47	383.79	0.26	1.41	2.44	11	0.277	1.685	0.829	18.8	0.232	0.0215	0.0642	1.96	10	151	245	132	75	1040	192	19	14	0	3	2.49
41	3	86	384.86	384.05		0.88	1.67	22.3	0.143	1.063	0.502	12.8	0.178	0.0156	0.0648	1.68	9	72	211	82	63	700	276	25	13	9	3	3.51
41	3	112	385.12	384.31	0.24	1.73	3.15	21.2	0.208	1.497	0.991	9.7	0.291	0.0253	0.0645	2.93	15	181	210	154	81	513	26	33	13	10	3	2.96
41	4	11	385.61	384.58	0.07	1.2	1.8	11.6	0.197	1.203	0.569	21.5	0.154	0.015	0.0642	1.35	6	89	228	113	48	1234	29	20	14	0	3	2.61
41	4	39	385.89	384.81	0.1	1.09	1.37	6.4	0.221	1.125	0.423	27	0.117	0.0111	0.064	0.92	5	66	237	105	39	1470	154	19	14	1	3	2.31
41	4	65	386.15	385.07	0.16	1.23	1.96	8.6	0.206	1.164	0.651	23.4	0.182	0.0143	0.064	1.5	9	99	232	105	50	1264	16	27	14	2	3	2.31
41	4	100	386.5	385.37	0.22	1.3	2.19	10.5	0.196	1.179	0.703	20.9	0.217	0.019	0.0639	1.82	9	88	229	96	52	1139	29	19	14	2	3	2.16
41	4	125	386.75	385.62	0.13	0.97	1.65	9.8	0.146	1.036	0.505	23.7	0.165	0.0136	0.0641	1.38	7	61	233	75	46	1300	162	20	14	3	3	2.41
41	5	5	387.05	385.88	0.22	1.27	2.34	12.2	0.204	1.341	0.753	19	0.226	0.0191	0.0641	1.93	11	112	225	109	55	1039	216	30	14	5	3	2.34
41	CC	10	387.27	386.1	0.23	1.25	2.19	11.7	0.228	1.365	0.699	20.1	0.207	0.0178	0.064	1.77	11	101	226	113	54	1096	78	30	14	0	3	2.26
41	CC	35	387.52	386.35	0.15	0.99	1.7	8	0.21	1.399	0.565	24.2	0.149	0.0133	0.0641	1.23	7	89	234	110	52	1391	30	24	14	1	3	2.41

Table 2. Hole 728B XRF data. * indicates unreliable trace element abundances.

Core no.	Sec. no.	Sec. depth (cm)	ODP depth (mbsf)	True depth (mbsf)	Na (%)	Mg (%)	Al (%)	Si (%)	P (%)	S (%)	K (%)	Ca (%)	Ti (%)	Cr (%)	Mn (%)	Fe (%)	Co (ppm)	Ni (ppm)	Cu (ppm)	Zn (ppm)	Rb (ppm)	Sr (ppm)	Ba (ppm)	La (ppm)	Pb (ppm)	Th (ppm)	U (ppm)	SALT (%)
20	4	25	178.55	178.55	0.01	1.81	2.20	11.50	0.043	0.555	0.727	21.5	0.192	0.0119	0.0640	1.82	11	33	229	63	40	1373	29	25	14	2	3	2.26
20	4	50	178.8	178.8		1.45	1.60	8.69	0.059	0.410	0.520	25.2	0.155	0.0122	0.0638	1.30	5	12	235	55	31	1517	176	39	14	0	3	2.01
20	4	75	179.05	179.05	0.01	1.66	1.83	8.85	0.072	0.585	0.611	24.2	0.168	0.0116	0.0639	1.50	8	30	233	72	35	1535	30	27	14	1	3	2.03
20	4	97	179.27	179.27	0.05	1.83	2.07	9.40	0.068	0.693	0.699	22.3	0.204	0.0143	0.0640	1.83	10	59	231	82	47	1233	79	21	14	3	3	2.19
20	4	125	179.55	179.55	0.13	2.19	2.59	11.50	0.064	0.719	0.884	19.2	0.249	0.0208	0.0638	2.29	12	77	227	88	58	1189	154	22	14	1	3	2
20	4	150	179.8	179.8	0.14	2.27	2.77	11.94	0.065	0.611	0.946	19.1	0.259	0.0198	0.0639	2.41	13	79	227	88	58	1205	672	26	13	3	3	2.03
20	5	25	180.05	180.05	0.13	2.12	2.74	12.45	0.057	0.682	0.929	18.8	0.253	0.0182	0.0638	2.39	14	72	225	82	55	1195	88	19	13	2	3	1.94
20	5	50	180.3	180.3	0.03	1.93	2.37	11.30	0.061	0.626	0.791	21.1	0.209	0.0111	0.0639	1.99	9	53	229	76	46	1410	334	19	14	0	3	2.14
20	5	75	180.55	180.55		1.39	1.48	7.45	0.060	0.496	0.474	26.9	0.120	0.0068	0.0641	1.09	8	12	238	68	32	1753	83	26	14	5	3	2.36
20	5	97	180.77	180.77		1.39	1.59	7.91	0.067	0.494	0.516	26.1	0.133	0.0078	0.0640	1.23	6	21	236	72	32	1691	30	32	14	0	3	2.23
20	5	125	181.05	181.05	0.02	1.65	1.92	8.79	0.081	0.609	0.653	24.4	0.164	0.0106	0.0640	1.56	7	38	234	83	40	1619	30	38	14	1	3	2.18
20	5	148	181.28	181.28	0.04	1.86	2.13	10.17	0.080	0.661	0.723	22.0	0.191	0.0137	0.0639	1.85	10	60	230	80	44	1473	568	25	14	4	3	2.15
20	6	25	181.55	181.55	0.14	2.07	2.48	12.10	0.079	0.693	0.839	19.3	0.237	0.0174	0.0639	2.18	13	76	226	77	46	1258	552	26	14	3	3	2.04
20	6	50	181.8	181.8	0.17	2.24	2.74	13.53	0.068	0.687	0.927	17.7	0.260	0.0215	0.0638	2.46	13	80	223	71	46	1125	810	36	13	2	3	1.92
20	6	75	182.05	182.05	0.21	2.37	3.02	13.99	0.053	0.721	1.023	16.6	0.281	0.0223	0.0637	2.65	13	88	222	68	50	1038	811	24	13	4	3	1.77
20	6	100	182.3	182.3	0.18	2.25	2.94	14.12	0.056	0.617	0.969	17.3	0.270	0.0196	0.0639	2.49	12	69	223	74	48	1170	847	21	13	1	3	2.13
20	6	125	182.55	182.55	0.12	2.15	2.73	13.67	0.055	0.626	0.899	18.5	0.233	0.0162	0.0637	2.26	13	60	223	78	46	1213	501	36	13	5	3	1.83
20	6	150	182.8	182.8		1.53	1.51	9.62	0.068	0.483	0.474	25.2	0.130	0.0087	0.0638	1.15	5	12	233	64	30	1584	30	39	14	3	3	1.97
27	5	25	247.75	247.75	0.07	1.66	1.81	8.31	0.046	0.387	0.599	25.7	0.151	0.0080	0.0636	1.38	8	20	235	71	31	1742	29	21	14	1	3	1.66
27	5	52	248.02	248.02		1.38	1.56	8.39	0.054	0.393	0.501	26.3	0.133	0.0070	0.0638	1.21	4	12	236	60	28	1779	30	25	14	0	3	1.93
27	5	75	248.25	248.25	0.04	1.60	1.82	9.16	0.069	0.437	0.608	24.6	0.155	0.0088	0.0638	1.40	7	42	234	81	33	1681	513	23	14	0	3	1.95
27	5	100	248.5	248.5	0.07	1.85	2.06	9.91	0.073	0.486	0.710	22.7	0.186	0.0116	0.0637	1.71	7	46	230	84	38	1569	29	21	14	5	3	1.77
27	5	125	248.75	248.75	0.10	1.97	2.39	10.68	0.070	0.534	0.842	20.8	0.230	0.0164	0.0637	2.02	8	62	228	78	41	1388	29	22	14	2	3	1.79
27	5	149	248.99	248.99	0.29	2.28	2.84	12.49	0.069	0.552	0.990	18.9	0.283	0.0213	0.0635	2.49	10	89	225	75	50	1230	1099	31	13	2	3	1.49
27	6	25	249.25	249.25	0.25	2.45	3.22	13.60	0.063	0.586	1.107	16.4	0.307	0.0214	0.0636	2.77	14	95	222	85	51	1097	840	21	13	1	3	1.67
27	6	50	249.5	249.5	0.26	2.40	3.28	13.71	0.058	0.644	1.127	16.9	0.301	0.0211	0.0636	2.91	13	87	223	82	54	1120	829	21	13	1	3	1.58
27	6	75	249.75	249.75	0.07	1.72	2.18	9.08	0.051	0.460	0.753	24.0	0.171	0.0084	0.0637	1.64	9	44	232	80	41	1697	29	20	14	5	3	1.83
27	6	100	250	250	0.00	1.44	1.75	7.81	0.057	0.402	0.584	26.3	0.140	0.0079	0.0638	1.28	5	32	237	71	31	1805	308	23	14	0	3	1.94
27	6	125	250.25	250.25	0.08	1.80	2.26	9.66	0.067	0.442	0.794	22.6	0.199	0.0150	0.0637	1.75	8	42	230	87	38	1592	616	38	14	1	3	1.82
27	6	150	250.5	250.5	0.33	2.66	3.46	14.71	0.083	0.665	1.167	15.3	0.321	0.0287	0.0635	2.98	15	126	219	99	57	1050	823	35	13	4	3	1.46
27	7	25	250.75	250.75	0.39	2.92	3.97	16.52	0.069	0.750	1.325	13.5	0.356	0.0300	0.0634	3.22	18	123	216	96	58	746	781	22	13	1	3	1.38
27	CC	4	250.95	250.95	0.20	2.16	2.95	12.44	0.051	0.468	1.002	19.1	0.254	0.0168	0.0635	2.33	10	51	224	71	47	1309	821	22	13	3	3	1.5
27	CC	30	251.2	251.2	0.15	2.09	2.26	10.09	0.052	0.355	0.731	23.0	0.186	0.0128	0.0635	1.72	10	37	229	58	37	1355	288	20	14	6	3	1.41
28	1	4	251.24	251.24	0.08	1.65	1.87	9.45	0.062	0.381	0.617	24.4	0.161	0.0094	0.0635	1.46	7	29	231	70	34	1688	67	23	14	2	3	1.41
28	1	26	251.46	251.46	0.06	1.60	1.63	8.37	0.061	0.327	0.518	26.0	0.142	0.0093	0.0636	1.22	5	25	235	68	26	1760	55	31	14	0	3	1.58
28	1	51	251.71	251.71	0.06	1.73	1.75	8.28	0.064	0.304	0.569	25.5	0.152	0.0098	0.0635	1.34	9	24	233	67	31	1697	137	22	14	3	3	1.45
28	1	76	251.96	251.96	0.09	2.08	2.18	9.83	0.080	0.519	0.738	22.1	0.205	0.0147	0.0636	1.78	8	56	229	83	38	1495	28	18	14	4	3	1.7
28	1	104	252.24	252.24	0.23	2.39	2.73	12.41	0.086	0.595	0.914	18.5	0.265	0.0221	0.0636	2.41	11	85	223	90	46	1230	540	18	13	1	3	1.56
28	1	126	252.46	252.46	0.21	2.45	2.69	12.08	0.075	0.554	0.910	18.9	0.256	0.0222	0.0636	2.32	11	72	225	85	42	1261	676	28	13	2	3	1.62
28	2	4	252.74	252.74	0.25	2.30	2.51	11.42	0.069	0.518	0.850	20.9	0.249	0.0164	0.0635	2.13	9	94	227	82	44	1327	981	31	13	3	3	1.47
28	2	26	252.96	252.96	0.21	2.27	2.50	11.79	0.077	0.512	0.843	20.8	0.248	0.0182	0.0637	2.07	8	82	227	79	45	1410	832	32	13	3	3	1.77
28	2	51	253.21	253.21	0.25	2.23	2.49	11.74	0.070	0.461	0.837	21.5	0.242	0.0151	0.0636	2.01	8	69	228	68	39	1421	89	33	13	2	3	1.63
28	2	76	253.46	253.46	0.23	2.23	2.66	11.88	0.062	0.453	0.908	20.7	0.257	0.0159	0.0635	2.29	10	84	228	75	43	1356	1170	31	13	1	3	1.55
28	2	104	253.74	253.74	0.25	2.25	2.71	12.47	0.068	0.439	0.917	20.3	0.257	0.0169	0.0636	2.22	9	84	227	79	45	1344	642	32	13	4	3	1.68
28	2	126	253.96	253.96	0.19	1.97	2.30	10.59	0.077	0.416	0.789	23.4	0.210	0.0119	0.0635	1.76	9	75	230	82	43	1575	267	32	13	7	3	1.5
28	3	4	254.24	254.24	0.21	2.14	2.52	12.52	0.099	0.418	0.853	20.9	0.246	0.0154	0.0636	2.01	9	77	227	83	39	1384	486	32	13	1	3	1.61
28	3	26	254.46	254.46	0.27	2.51	3.19	15.23	0.087	0.519	1.048	16.8	0.297	0.0201	0.0636	2.62	11	100	221	88	50	1162	1180	31	13	4	3	1.69
28	3	51	254.71	254.71	0.23	2.38	2.98	14.04	0.074	0.479	0.989	18.5	0.274	0.0184	0.0636	2.41	11	104	224	86	48	1280	1052	32	13	2	3	1.65
28	3	76	254.96	254.96	0.12	1.64	1.53	8.37	0.061	0.297	0.475	28.0	0.140	0.0072	0.0635	1.13	3	25	238	46	24	1786	703	34	14	1	3	1.52
28	3	101	255.21	255.21	0.10	1.89	1.78	9.25	0.064	0.341	0.567	26.0	0.169	0.0102	0.0637	1.38	5	42	234	68	30	1722	481	34	14	1	3	1.82
28	3	126	255.46	255.46	0.23	2.48	2.40	11.05	0.081	0.516	0.783	21.8	0.227	0.0166	0.0635	1.90	9	102	228	83	40	1425	189	33	13	2	3	1.55
28	4	1	255.71	255.71	0.44	3.21	3.47	16.08	0.093	0.657	1.107	14.9	0.338	0.0308	0.0635	2.92	14	153	217	97	50	819	1047	30	13	2	3	1.41
28	4	26	255.96	255.96	0.41	3.18	3.76	16.82	0.070	0.723	1.223	14.3	0.346	0.0304	0.0635	3.14	15	159	216	133	54	775	948	30	13	3	3	1.52
28	4	51	256.21	256.21	0.08	1.17	1.15	6.22	0.066	0.370	0.343	30.6	0.109	0.0032	0.0636	0.86	2	26	242	60	23	1944	1044	35	14	2	3	1.64
28	4	76	256.46	256.46	0.05	1.65	1.34	8.29	0.047	0.193	0.394	28.6	0.119	0.0053	0.0635	0.89	0	12	237	27	22	1867	456	33	14	1	3	1.43
28	4	101	256.71	256.71	0.09	2.09	1.65	9.42	0.069	0.274	0.488	26.4	0.153	0.0086	0.0637	1.18	2	24	234	96	26	1737	132	34	14	0	3	1.75
28	4	126	256.96	256.96	0.22	2.33	2.31	12.43	0.081	0.437	0.747	21.5	0.223	0.0159	0.0636	1.85	7	71	227	73	33	1459	501	32	13	0	3	1.68
28	5	1	257.21	257.21	0.29	2.41	2.56	12.98	0.093	0.500	0.844	19.4	0.270	0.0225	0.0636	2.13	8	79	225	77	40	1312	1129	31	13	0	3	1.57
28	5	26	257.46	257.46	0.32	2.48	2.98	13.50	0.077	0.533	0.979	18.1	0.299	0.0214	0.0635	2.52	9	91	223	73	43	1207	1052	31	13	0	3	1.41
28	5	51	257.71	257.71	0.14	1.57	1.54	8.50	0.064	0.275	0.470	28.4	0.141	0.0069	0.0636	1.02	3	14	238	51	19	1830	1008	34	14	0	3	1.65
28	5	76	257.96	257.96	0.15	1.68	1.73	8.79	0.064	0.355	0.569	26.0	0.173	0.0096	0.0634	1.40	6	54	234	63	28	1693	777	33	14	2	3	1.37
28	5	101	258.21	258.21	0.08	1.48	1.47	6.75	0.057	0.357	0.483	28.4	0.148	0.0067	0.0635	1.17	3	35	240	60	23	1870	717	35	14	0	3	1.52
28	5	126	258.46	258.46	0.26	2.32	2.54	11.74	0.083	0.504	0.845	20.3	0.263	0.0232	0.0635	2.09	7	85	225	75	37	1350	126	31	13	0	3	1.48
28	6	1	258.71	258.71	0.33	2.67	3.39	14.58	0.059	0.610	1.109	16.7	0.315	0.0242	0.0634	2.82	14	135	221	91	46	1165	1170	30	13	1	3	1.39
28	6	26	258.96	258.96	0.08	1.22	1.33	6.80	0.065	0.339	0.414	29.7	0.123	0.0065	0.0635	0.98	4	38	241	65	18	1923	946	35	14	0	3	1.49
28	6	51	259.21	259.21	0.10	1.42	1.54	8.09	0.085	0.400	0.484	28.0	0.148	0.0069	0.0637	1.15	3	44	238	67	25	1822	854	34	14	0	3	1.77
28	6	76	259.46	259.46	0.19	1.85	2.17	10.35	0.080	0.503	0.726	23.4	0.213	0.0136	0.0635	1.82	8	83	232	81	34	1545	981	33	14	0	3	1.55
28	6	101	259.71	259.71	0.18	1.82	2.11	10.52	0.077	0.484	0.706	23.4	0.205	0.0129	0.0636	1.76	6	72	232	70	29	1532	847	33	14	0	3	1.57

28	6	126	259.96	259.96	0.09	1.38	1.53	9.69	0.057	0.394	0.492	26.6	0.138	0.0052	0.0636	1.20	3	39	235	60	24	1754	916	34	14	0	3	1.65
28	7	1	260.21	260.21	0.21	2.23	2.69	12.52	0.048	0.402	0.905	20.5	0.242	0.0161	0.0635	2.13	10	81	225	72	39	1335	223	31	13	1	3	1.44
28	7	26	260.46	260.46	0.12	1.71	1.78	8.52	0.060	0.472	0.584	25.8	0.173	0.0102	0.0637	1.44	4	51	235	70	23	1662	1040	34	14	0	3	1.77
28	CC	9	260.69	260.69	0.27	2.13	2.38	11.76	0.063	0.549	0.795	21.1	0.236	0.0165	0.0635	2.03	10	95	227	85	38	1345	914	31	13	5	3	1.44
29	1	10	260.9	260.9	0.24	2.15	2.58	13.02	0.101	0.480	0.881	20.3	0.253	0.0175	0.0636	2.05	8	76	225	80	57	1383	247	32	27	8	3	1.67
29	1	35	261.15	261.15	0.34	2.32	2.98	14.62	0.100	0.521	1.005	17.6	0.295	0.0209	0.0635	2.41	9	81	221	77	74	1225	1209	31	46	16	3	1.45
29	1	60	261.4	261.4	0.35	2.46	3.29	15.79	0.092	0.588	1.117	16.2	0.323	0.0219	0.0635	2.68	11	98	219	82	359	1156	1100	30	176	45	40	1.48
29	1	85	261.65	261.65	0.25	2.34	3.14	15.36	0.073	0.517	1.048	17.7	0.281	0.0173	0.0636	2.49	11	100	222	80	358	1241	897	32	175	44	48	1.68
29	1	110	261.9	261.9	0.15	1.52	1.72	9.51	0.066	0.397	0.572	26.1	0.157	0.0076	0.0635	1.35	3	41	235	58	360	1582	989	34	177	44	14	1.54
29	1	135	262.15	262.15	0.13	1.42	1.50	8.85	0.063	0.328	0.466	27.6	0.143	0.0077	0.0636	1.14	4	39	237	55	359	1652	593	34	177	44	7	1.64
29	2	10	262.4	262.4	0.18	1.91	1.90	9.62	0.073	0.474	0.617	25.0	0.181	0.0106	0.0636	1.51	5	56	233	69	360	1544	42	33	177	44	22	1.7
29	2	35	262.65	262.65	0.26	2.43	2.35	11.75	0.088	0.620	0.772	20.8	0.239	0.0181	0.0637	2.07	7	93	227	84	358	1337	585	33	179	45	48	1.74
29	2	60	262.9	262.9	0.38	2.88	3.19	15.48	0.082	0.782	1.045	16.0	0.313	0.0249	0.0636	2.96	13	133	220	98	357	1045	364	30	176	45	44	1.63
29	2	85	263.15	263.15	0.42	2.80	3.47	16.65	0.068	0.705	1.150	14.9	0.327	0.0260	0.0635	3.09	13	141	217	89	355	1005	623	30	174	44	48	1.51
29	2	110	263.4	263.4	0.30	2.49	3.12	15.10	0.064	0.539	1.035	17.4	0.286	0.0203	0.0637	2.58	11	100	222	81	357	1224	753	31	175	44	43	1.72
29	2	135	263.65	263.65	0.15	1.38	1.50	9.10	0.084	0.375	0.454	27.5	0.143	0.0078	0.0638	1.09	4	33	237	59	357	1650	921	34	175	43	9	1.91
29	3	10	263.9	263.9		1.49	1.65	9.26	0.098	0.471	0.560	25.0	0.140	0.0134	0.0637	1.28	50	221	318	210	17	1583	136	31	14	0	3	1.81
29	3	35	264.15	264.15	0.19	1.83	2.23	12.66	0.085	0.487	0.760	21.7	0.210	0.0117	0.0637	1.76	5	67	227	73	357	1455	201	32	175	44	35	1.72
29	3	60	264.4	264.4	0.11	1.57	1.82	10.92	0.096	0.434	0.595	24.7	0.172	0.0095	0.0638	1.39	3	35	233	59	357	1593	451	34	176	43	28	1.94
29	3	85	264.65	264.65	0.15	1.44	1.66	9.83	0.095	0.420	0.544	25.8	0.173	0.0091	0.0637	1.27	4	32	234	69	358	1590	925	34	176	43	11	1.79
29	3	110	264.9	264.9	0.21	1.81	2.14	11.02	0.072	0.442	0.719	23.4	0.217	0.0132	0.0637	1.70	7	68	230	73	359	1523	272	33	175	43	14	1.82
29	3	135	265.15	265.15	0.23	2.04	2.46	11.48	0.064	0.484	0.842	21.4	0.249	0.0184	0.0637	2.06	8	77	229	71	362	1469	1244	32	176	44	29	1.81
29	4	10	265.4	265.4	0.32	2.19	2.81	12.95	0.062	0.555	0.947	19.6	0.270	0.0198	0.0635	2.41	10	88	225	73	360	1324	827	31	175	44	15	1.53
29	4	35	265.65	265.65	0.26	2.00	2.58	12.21	0.063	0.493	0.882	21.4	0.238	0.0140	0.0636	2.04	9	73	228	73	359	1418	164	33	175	44	18	1.6
29	4	60	265.9	265.9	0.19	1.67	1.94	10.18	0.088	0.399	0.644	25.1	0.184	0.0135	0.0637	1.48	5	43	233	67	358	1556	387	34	176	43	8	1.73
29	4	85	266.15	266.15*		1.87	2.16	10.00	0.091	0.520	0.765	22.4	0.187	0.0183	0.0637	1.79	63	253	327	223	17	1348	28	20	14	0	3	1.72
29	4	110	266.4	266.4 *	0.07	2.46	2.99	13.63	0.088	0.579	1.052	17.1	0.275	0.0280	0.0635	2.53	65	291	308	221	17	1028	343	18	13	0	3	1.44
29	4	135	266.65	266.65*	0.21	2.89	3.80	16.68	0.064	0.511	1.327	13.8	0.333	0.0326	0.0634	3.05	65	292	289	224	16	679	26	22	13	0	3	1.29
29	5	10	266.9	266.9 *		1.81	2.23	11.77	0.079	0.473	0.793	21.4	0.200	0.0215	0.0635	1.77	63	244	303	210	17	1325	28	19	14	0	3	1.55
29	5	35	267.15	267.15*	0.02	2.16	2.64	13.10	0.081	0.472	0.928	19.4	0.237	0.0243	0.0634	2.20	64	278	322	221	17	1137	27	19	13	0	3	1.35
29	5	60	267.4	267.4 *	0.08	2.40	2.85	14.09	0.092	0.655	0.990	17.1	0.264	0.0279	0.0635	2.50	65	308	324	243	17	1032	27	36	13	0	3	1.55
29	5	85	267.65	267.65*	0.19	2.71	3.37	17.13	0.061	0.633	1.148	14.0	0.315	0.0309	0.0018	3.00	67	320	306	232	16	507	26	33	13	0	3	1.34
29	5	110	267.9	267.9 *		2.11	2.68	13.59	0.051	0.444	0.944	18.7	0.233	0.0203	0.0634	2.22	64	249	294	214	17	1142	27	22	13	0	3	1.31
29	5	135	268.15	268.15*		2.02	2.25	12.92	0.101	0.397	0.758	20.7	0.203	0.0241	0.0635	1.76	62	241	311	214	17	1279	27	22	13	0	3	1.55
29	6	10	268.4	268.4 *		2.11	2.30	12.15	0.097	0.524	0.790	19.8	0.221	0.0229	0.0635	2.01	62	266	306	210	17	1229	27	29	14	0	3	1.48
29	6	35	268.65	268.65*		2.25	2.47	12.59	0.085	0.515	0.854	19.2	0.230	0.0236	0.0634	2.15	63	268	308	216	17	1178	27	29	14	0	3	1.34
29	6	60	268.9	268.9 *		2.05	2.20	11.63	0.072	0.425	0.756	21.0	0.198	0.0218	0.0635	1.86	64	249	307	208	17	1332	41	37	14	0	3	1.5
29	6	85	269.15	269.15*		1.70	1.61	8.79	0.069	0.332	0.539	25.4	0.128	0.0140	0.0634	1.36	63	222	309	203	17	1564	29	39	14	0	3	1.39
29	6	110	269.4	269.4 *		2.25	2.12	10.93	0.074	0.466	0.728	21.3	0.205	0.0232	0.0635	1.83	62	256	305	213	17	1357	28	37	14	0	3	1.51
29	6	135	269.65	269.65*	0.07	2.54	2.75	13.33	0.063	0.486	0.938	18.1	0.248	0.0272	0.0635	2.36	64	265	303	215	17	1179	542	25	13	0	3	1.53
29	7	10	269.9	269.9 *	0.09	2.58	3.22	14.61	0.066	0.531	1.119	16.4	0.277	0.0255	0.0635	2.65	65	281	292	226	17	1037	26	21	13	0	3	1.47
29	7	35	270.15	270.15*		1.45	1.59	8.47	0.064	0.408	0.561	25.3	0.131	0.0139	0.0636	1.30	61	217	309	208	17	1587	29	21	14	0	3	1.59
29	CC	16	270.37	270.37*		1.64	1.80	9.49	0.057	0.401	0.646	23.8	0.159	0.0167	0.0634	1.51	61	213	297	198	17	1609	28	20	14	0	3	1.38
29	CC	41	270.62	270.62*		1.84	1.98	9.28	0.045	0.411	0.715	23.2	0.184	0.0174	0.0633	1.79	65	247	309	199	17	1428	352	30	14	0	3	1.17
30	1	10	270.6	270.6 *		1.46	1.31	7.67	0.054	0.291	0.432	27.4	0.099	0.0109	0.0634	1.00	61	187	292	182	18	1563	56	21	14	0	3	1.31
30	1	35	270.85	270.85*		1.89	1.89	9.35	0.055	0.376	0.664	23.7	0.163	0.0190	0.0633	1.58	62	225	304	216	17	1438	28	18	14	0	3	1.19
30	1	60	271.1	271.1 *		2.25	2.21	10.98	0.061	0.490	0.776	21.1	0.210	0.0229	0.0636	1.92	62	245	309	237	17	1428	28	19	14	0	3	1.56
30	1	85	271.35	271.35*	0.11	2.53	3.05	14.47	0.052	0.581	1.061	16.4	0.283	0.0316	0.0633	2.68	65	276	297	216	17	1008	230	34	13	0	3	1.22
30	1	110	271.6	271.6 *		1.82	1.95	10.63	0.080	0.394	0.675	22.6	0.193	0.0209	0.0634	1.57	60	216	309	197	17	1391	388	24	14	0	3	1.39
30	1	135	271.85	271.85*		2.00	2.22	12.00	0.071	0.505	0.779	20.1	0.228	0.0286	0.0635	1.94	62	241	299	210	17	1273	27	23	14	0	3	1.49
30	2	10	272.1	272.1 *	0.05	2.38	2.89	14.51	0.048	0.545	1.019	16.6	0.275	0.0294	0.0634	2.54	64	276	290	214	17	984	26	34	13	0	3	1.25
30	2	35	272.35	272.35*		1.51	1.54	9.67	0.062	0.317	0.521	25.0	0.140	0.0170	0.0635	1.21	60	201	301	189	17	1546	321	23	14	0	3	1.41
30	2	60	272.6	272.6 *		1.78	1.91	10.04	0.066	0.460	0.667	22.9	0.179	0.0195	0.0635	1.66	62	232	314	210	17	1433	260	23	14	0	3	1.5
30	2	85	272.85	272.85*	0.12	2.41	2.76	15.31	0.064	0.688	0.945	16.1	0.279	0.0298	0.0636	2.61	65	300	310	231	17	990	26	35	13	0	3	1.62
30	2	110	273.1	273.1 *	0.08	2.58	3.14	16.08	0.043	0.553	1.087	15.6	0.273	0.0263	0.0634	2.72	66	285	304	216	16	953	26	34	13	0	3	1.31
30	2	135	273.35	273.35*		1.74	1.78	10.58	0.067	0.416	0.621	23.2	0.166	0.0157	0.0635	1.47	61	220	310	199	17	1458	28	38	14	0	3	1.55
30	3	10	273.6	273.6 *		1.90	2.12	11.93	0.054	0.471	0.768	20.5	0.203	0.0215	0.0635	1.83	62	234	299	203	17	1208	28	37	14	0	3	1.53
30	3	35	273.85	273.85*		2.03	2.15	11.77	0.058	0.435	0.757	20.9	0.201	0.0196	0.0635	1.83	62	238	313	208	17	1238	28	19	14	0	3	1.54
30	3	60	274.1	274.1 *	0.02	2.15	2.28	12.04	0.053	0.428	0.777	20.2	0.204	0.0203	0.0635	1.89	62	229	291	204	17	1264	27	19	14	0	3	1.52
30	3	85	274.35	274.35*		1.89	2.00	10.63	0.053	0.388	0.707	22.5	0.166	0.0147	0.0633	1.67	63	228	314	206	17	1441	28	37	14	0	3	1.23
30	3	110	274.6	274.6 *		1.64	1.64	11.21	0.066	0.324	0.552	23.6	0.142	0.0129	0.0636	1.29	59	194	291	192	17	1489	224	24	14	0	3	1.63
30	3	135	274.85	274.85*		1.80	1.92	12.19	0.066	0.403	0.658	21.9	0.178	0.0167	0.0637	1.62	61	220	300	201	17	1444	29	24	14	0	3	1.79
30	4	10	275.1	275.1 *		1.82	2.10	13.20	0.052	0.457	0.738	19.8	0.200	0.0199	0.0635	1.94	63	245	293	204	17	1242	27	29	14	0	3	1.5
30	4	35	275.35	275.35*	0.01	2.05	2.57	15.68	0.035	0.477	0.895	17.0	0.241	0.0232	0.0635	2.35	66	256	303	210	17	1055	26	21	13	0	3	1.52
30	4	60	275.6	275.6 *		1.86	2.21	12.94	0.034	0.448	0.778	20.2	0.192	0.0174	0.0634	1.96	64	241	292	199	17	1313	41	22	14	0	3	1.35
30	4	85	275.85	275.85*		1.65	1.62	9.95	0.044	0.363	0.544	24.5	0.139	0.0125	0.0638	1.32	61	191	289	181	17	1593	332	31	14	0	3	1.87
30	4	110	276.1	276.1 *		1.47	1.50	9.60	0.050	0.334	0.512	24.8	0.133	0.0128	0.0635	1.35	60	195	302	188	17	1614	119	30	14	0	3	1.5
30	4	135	276.35	276.35*		2.05	2.27	12.05	0.058	0.543	0.797	20.0	0.229	0.0239	0.0635	2.06	64	258	309	219	17	1270	27	29	14	0	3	1.53
30	5	10	276.6	276.6 *	0.24	2.68	3.30	17.01	0.045	0.629	1.122	14.0	0.322	0.0342	0.0636	2.96	67	295	306	226	16	856	530	22	13	0	3	1.68
30	5	35	276.85	276.85*	0.07	1.44	1.72	9.21	0.056	0.378	0.600	24.6	0.157	0.0110	0.0636	1.36	6	12	233	62	36	1646	550	21	14	4	3	1.61
30	5	60	277.1	277.1 *	0.18	1.90	2.30	12.23	0.058	0.550	0.797	19.7	0.233	0.0166	0.0635	2.04	10	65	224	74	46	1387	27	23	14	6	3	1.48
30	5	85	277.35	277.35*	0.24	2.21	2.82	14.78	0.052	0.517	0.963	17.2	0.272	0.0208	0.0635	2.42	12	87	220	80	46	1138	414	28	13	1	3	1.49
30	5	108	277.58	277.58*		1.25	1.27	8.22	0.061	0.307	0.411	27.4	0.114	0.0133	0.0636	1.01	59	180	290	179	18	1678	257	23	14	0	3	1.68

Table 3. Site 731 XRF data. * indicates unreliable trace element abundances.

Core no.	Sec no.	Sec depth (cm)	ODP depth (mbsf)	True depth (mbsf)	Na (%)	Mg (%)	Al (%)	Si (%)	P (%)	S (%)	K (%)	Ca (%)	Ti (%)	Cr (%)	Mn (%)	Fe (%)	Co (ppm)	Ni (ppm)	Cu (ppm)	Zn (ppm)	Rb (ppm)	Sr (ppm)	Ba (ppm)	La (ppm)	Pb (ppm)	Th (ppm)	U (ppm)	Salt (%)
Hole 731A																												
32	1	33	299.53	299.53*	0.25	1.31	2.11	7.6	0.007	0.017	0.883	28.3	0.143	0	0.0146	1.5	5	12	239	32	32	1439	417	27	14	0	3	0.69
32	1	60	299.8	299.8 *	0.22	1.54	1.89	7	0	0.021	0.741	29.2	0.126	0	0.0157	1.32	7	12	238	40	27	1225	69	28	14	0	3	0.59
32	1	90	300.1	300.1 *	0.29	2.47	3.07	12.2	0.003	0.032	1.216	21	0.227	0.0048	0.0149	2.36	12	25	227	54	44	1290	189	19	13	3	3	0.74
32	1	120	300.4	300.4 *	0.17	0.81	1.16	3.9	0	0.014	0.425	34.1	0.073	0	0.0011	0.67	1	13	247	7	18	1393	31	22	14	0	3	0.61
32	1	149	300.69	300.69*	0.2	0.93	1.65	5.5	0	0.014	0.637	31.8	0.101	0	0.0017	1.07	1	13	244	16	26	1352	291	32	14	0	3	0.81
32	2	30	301	301 *	0.16	0.9	1.29	4.5	0	0.017	0.468	33.3	0.086	0	0.0074	0.83	3	13	246	10	20	1279	31	32	14	1	3	0.83
32	2	60	301.3	301.3 *	0.33	2.49	3.36	13.3	0	0.033	1.363	19.5	0.264	0.0062	0.0073	2.72	15	59	225	61	52	1263	51	35	13	2	3	0.69
32	2	90	301.6	301.6 *	0.24	1.12	1.95	6.9	0	0.018	0.779	29.5	0.139	0	0.0038	1.43	6	12	240	34	31	1258	329	39	14	0	3	0.56
32	2	120	301.9	301.9 *	0.32	1.44	2.5	9.4	0.005	0.031	1.054	25.8	0.194	0.0007	0.0099	2.05	11	12	235	59	36	1250	41	30	14	0	3	0.52
32	2	149	302.19	302.19*	0.21	1.94	2.41	9.3	0.001	0.03	0.91	25.8	0.175	0.0015	0.0157	1.88	8	12	235	79	31	1132	368	27	14	0	3	0.72
32	3	30	302.5	302.5 *	0.17	1.15	1.83	6.5	0	0.016	0.736	29.9	0.121	0	0.063	1.29	8	12	241	41	26	1363	30	28	14	0	3	0.64
32	3	60	302.8	302.8 *	0.15	0.97	1.64	5.5	0	0.014	0.664	31.7	0.11	0	0.0056	1.08	5	13	244	17	22	1179	30	23	14	0	3	0.78
32	3	88	303.08	303.08*	0.18	0.98	1.64	5.6	0	0.016	0.657	31.5	0.108	0	0.0084	1.06	4	13	243	34	25	1186	30	24	14	0	3	0.62
32	3	118	303.38	303.38*	0.34	1.78	3.52	12.4	0.012	0.013	1.445	21	0.24	0.0046	0.0124	2.63	14	12	227	68	56	1100	27	22	13	0	3	0.57
32	3	150	303.7	303.7 *	0.24	1.33	2.34	8.2	0.001	0.012	0.995	27.2	0.165	0	0.0058	1.73	5	12	236	27	36	1184	29	27	14	2	3	0.55
32	4	33	304.03	304.03*		1.31	2.14	7.9	0.005	0.02	0.928	27.9	0.145	0.0047	0.0204	1.68	62	172	311	180	18	1096	29	27	14	0	3	0.51
32	4	60	304.3	304.3 *	0.01	2.45	3.16	12.3	0.005	0.024	1.315	20.9	0.229	0.01	0.0357	2.57	65	192	300	190	17	978	27	36	13	0	3	0.66
32	4	90	304.6	304.6 *		1.31	2.19	8	0.002	0.018	0.946	27.7	0.147	0.0042	0.0155	1.67	63	172	311	176	18	1247	29	38	14	0	3	0.5
32	4	120	304.9	304.9 *		0.86	1.27	4.6	0	0.016	0.553	32.9	0.087	0.0016	0.013	0.98	59	141	311	157	18	1224	31	23	14	0	3	0.48
32	4	149	305.19	305.19*		0.83	1.17	4.1	0	0.017	0.46	33.9	0.071	0.001	0.016	0.81	58	131	304	144	18	1203	31	22	14	0	3	0.53
32	5	30	305.5	305.5 *		1.72	2.16	8	0	0.02	0.875	27.4	0.142	0.0057	0.033	1.58	60	168	293	162	18	1130	81	23	14	0	3	0.47
32	5	60	305.8	305.8 *		1.37	1.88	6.9	0	0.02	0.785	29.1	0.124	0.0042	0.0206	1.29	61	171	341	175	18	1345	30	22	14	0	3	0.47
32	5	90	306.1	306.1 *		0.71	0.97	3.2	0	0.016	0.358	35	0.053	0.0008	0.0255	0.6	59	145	304	146	18	1305	31	23	14	0	3	0.87
32	5	120	306.4	306.4 *		0.72	1.02	3.3	0	0.016	0.387	34.7	0.059	0.0013	0.0312	0.64	59	136	299	151	18	1291	31	21	14	0	3	0.82
32	5	149	306.69	306.69*		0.57	0.74	2.3	0	0.013	0.259	36.7	0.042	0	0.0235	0.46	57	118	290	135	18	1306	32	23	14	0	3	0.61
32	6	30	307	307 *		0.55	0.68	2.1	0	0.014	0.211	37.1	0.036	0	0.0249	0.41	58	138	291	135	18	1283	32	22	14	0	3	0.75
32	6	60	307.3	307.3 *		0.62	0.81	2.6	0	0.016	0.268	36.1	0.044	0.0011	0.0281	0.5	59	131	323	145	18	1281	32	29	14	0	3	0.65
32	6	90	307.6	307.6 *	0.39	2.75	5.76	20.9	0.023	0.015	2.261	9.4	0.406	0.0175	0.039	4.61	73	270	290	264	16	504	177	31	12	0	3	0.53
32	6	120	307.9	307.9 *		0.69	0.91	3	0	0.015	0.331	35.5	0.049	0.0005	0.0291	0.56	57	131	284	141	18	1295	31	41	14	0	3	0.55
32	CC	30	308.5	308.5 *	0.16	0.7	1.06	3.4	0	0.013	0.366	35.1	0.069	0	0.015	0.66	0	13	249	3	18	1324	59	33	14	0	3	0.61
37	1	30	341.6	341.6 *	0.49	3.25	7.43	24.4	0.024	0.014	2.815	4.3	0.52	0.0238	0.1697	6.11	79	329	316	290	15	257	22	18	12	0	3	0.57
37	1	60	341.9	341.9 *	0.53	3.38	7.72	25	0.025	0.014	2.941	2.7	0.535	0.0254	0.2723	7.02	84	343	342	291	15	124	22	17	12	0	2	0.59
37	1	90	342.2	342.2 *	0.35	2.64	5.35	18.2	0.029	0.022	2.042	12	0.389	0.0162	0.2577	5.09	74	238	309	233	16	983	123	23	13	0	3	0.68
37	1	120	342.5	342.5 *	0.15	2.56	4.61	16.2	0.012	0.021	1.78	14.8	0.321 *	0.0128	0.4328	3.6	51	231	289	226	16	1054	71	27	13	0	3	0.63
37	1	150	342.8	342.8 *	0.43	3.11	6.93	22.6	0.02	0.014	2.7	6.1	0.465	0.022	0.199	6.09	66	317	309	273	16	329	242	21	12	0	3	0.56
37	2	30	343.1	343.1 *	0.44	3.4	7.75	23.6	0.013	0.013	3.084	3.9	0.492	0.0256	0.1672	6.87	70	347	301	295	15	158	22	15	12	0	3	0.58
37	2	60	343.4	343.4 *	0.48	3.5	6.71	22.3	0.019	0.017	2.594	6.6	0.464	0.0252	0.2203	5.76	66	327	298	288	16	313	23	15	12	0	3	0.59
37	2	90	343.7	343.7 *	0.41	2.82	6.34	20.7	0.029	0.019	2.463	8.5	0.432	0.0191	0.2626	5.72	63	279	332	259	16	537	97	16	12	0	3	0.59
37	2	120	344	344 *	0.65	3.27	7.57	25.7	0.024	0.013	2.78	3	0.552	0.0263	0.2479	6.19	84	335	312	295	15	111	41	16	12	0	2	0.51
37	2	150	344.3	344.3 *	0.53	3.22	7.41	24.1	0.027	0.014	2.794	4	0.508	0.0228	0.2198	6.58	82	311	361	280	15	252	22	21	12	0	3	0.57
37	3	30	344.6	344.6 *	0.61	3.53	8.08	25.7	0.029	0.013	3.039	1.7	0.55	0.0261	0.2479	7.41	87	339	383	298	15	62	50	20	12	0	2	0.65
37	3	60	344.9	344.9 *	0.6	3.17	7.14	24.9	0.032	0.015	2.605	4.1	0.526	0.0229	0.1696	5.88	80	297	317	302	15	224	22	29	12	0	3	0.56
37	3	90	345.2	345.2 *	0.64	3.01	6.78	26	0.041	0.012	2.384	4	0.534	0.0237	0.1261	5.05	75	286	277	293	15	100	114	29	12	0	3	0.37
37	3	120	345.5	345.5 *	0.5	3.14	5.55	19.4	0.019	0.024	1.973	11.2	0.403	0.0163	0.3495	4.51	74	249	308	243	16	951	593	15	12	0	3	0.91
37	3	149	345.79	345.79*	0.93	3.18	6.23	25.3	0.06	0.015	2.278	5.4	0.559	0.0239	0.1588	4.66	73	256	323	276	15	194	257	14	12	0	3	0.54
37	4	30	346.1	346.1 *	0.46	2.63	6.12	20.1	0.033	0.019	2.291	9.8	0.426	0.0173	0.2861	5.35	77	264	375	258	16	611	434	25	12	0	3	0.74
37	4	60	346.4	346.4 *	0.45	3.38	7.73	24.6	0.025	0.013	2.963	3.7	0.517	0.0243	0.1869	6.56	82	343	369	293	15	111	22	19	12	0	2	0.55
37	4	88	346.68	346.68*	0.55	3.1	7.22	23.4	0.034	0.015	2.634	5.1	0.511	0.0226	0.3345	6.5	83	305	349	282	15	406	401	15	12	0	3	0.68
37	5	30	347.6	347.27*	0.57	3.4	7.58	25.5	0.027	0.013	2.835	3.1	0.527	0.0249	0.2551	6.29	81	324	384	294	15	87	22	14	12	0	2	0.56
37	5	59	347.89	347.56*	0.38	3.12	5.77	20.4	0.027	0.023	2.161	9.1	0.414	0.0185	0.3964	5.15	77	271	366	252	16	570	576	19	13	0	3	0.68
37	5	90	348.2	347.87*	0.51	3.3	7.55	24.8	0.024	0.013	2.904	3.5	0.521	0.0243	0.1317	6.54	83	326	305	294	15	101	22	29	12	0	3	0.49
37	5	120	348.5	348.17*	0.53	3.09	7.12	23.4	0.014	0.015	2.745	5.6	0.485	0.0227	0.2227	5.81	82	328	319	288	15	331	23	30	12	0	3	0.54

37	5	149	348.79	348.46*	0.63	3.24	7.08	23.3	0.037	0.017	2.669	5.4	0.501	0.0221	0.1922	6.28	82	301	317	287	15	393	331	24	12	0	3	0.78
37	6	30	349.1	348.77*	0.41	3.16	5.4	19.4	0.031	0.026	1.942	10.8	0.393	0.0174	0.3485	4.71	74	259	315	246	16	827	509	22	12	0	3	0.71
37	6	60	349.4	349.07*	0.52	3.1	6.23	21.4	0.034	0.021	2.434	7.9	0.437	0.019	0.1905	5.81	79	287	372	266	16	496	552	25	12	0	3	0.64
37	6	90	349.7	349.37*	0.33	2.24	4.78	16.2	0.024	0.02	1.828	15.4	0.327	0.0133	0.2735	3.8	69	221	300	223	16	1213	26	34	13	0	3	0.61
37	6	120	350	349.67*	0.37	2.69	5:56	19.2	0.028	0.022	2.084	10.9	0.392	0.0177	0.2681	4.93	75	281	371	252	16	817	600	32	13	0	3	0.59
37	6	149	350.29	349.96*	0.62	3.23	6.53	22.9	0.028	0.021	2.362	5.9	0.493	0.0227	0.2029	5.87	82	322	317	287	16	489	569	30	12	0	3	0.75
37	7	28	350.58	350.25*	0.36	2.37	4.85	17	0.032	0.017	1.729	13.7	0.36	0.0144	0.2814	4.43	74	244	350	244	16	1057	25	23	13	0	3	0.64
38	1	25	351.25	351.25*	0.5	3.18	6.94	23.3	0.025	0.018	2.72	5.6	0.49	0.0223	0.0895	6.17	80	303	304	271	15	442	157	16	12	0	3	0.69
38	1	55	351.55	351.55*	0.54	3.17	7.24	24.9	0.017	0.018	2.839	3.9	0.499	0.0232	0.0637	6.13	82	319	288	272	15	156	22	14	12	0	3	0.51
38	1	85	351.85	351.85*	0.57	3.23	7.23	25.8	0.022	0.018	2.718	3.3	0.515	0.0238	0.0534	5.94	79	322	314	311	15	151	71	14	12	0	2	0.62
38	1	115	352.15	352.15*	0.51	3.13	6.67	23.2	0.021	0.02	2.577	6.2	0.492	0.0212	0.076	5.51	78	271	313	276	15	543	284	16	12	0	3	0.72
38	1	145	352.45	352.45*	0.54	3.17	7.25	25	0.025	0.015	2.794	3.8	0.517	0.0238	0.0733	6.23	80	310	295	291	15	283	22	19	12	0	3	0.62
38	2	25	352.75	352.75*	0.58	3.54	7.66	25.9	0.038	0.017	2.966	1.9	0.566	0.0262	0.0651	7.34	86	331	302	306	15	90	22	23	12	0	2	0.77
38	2	55	353.05	353.05*	0.51	3.57	7.04	25.1	0.029	0.02	2.705	3.6	0.551	0.0249	0.0766	6.31	81	312	336	284	15	264	22	20	12	0	3	0.81
38	2	85	353.35	353.35*		1.47	2.57	8.8	0.047	0.054	0.945	26.5	0.185	0.0059	0.2197	1.72	61	172	891	185	17	1169	29	27	14	0	3	0.76
38	2	115	353.65	353.65*	0.13	2.11	3.89	14.1	0.028	0.016	1.684	18.1	0.273	0.0115	0.3024	3.22	67	203	303	212	17	1249	27	28	13	0	3	0.62
38	2	145	353.95	353.95*	0.45	3.21	5.93	21.2	0.018	0.016	2.584	7.9	0.409	0.0206	0.1216	5.67	79	283	295	264	16	404	23	31	12	0	3	0.68
38	3	25	354.25	354.25*	0.48	3.35	7.52	24.9	0.03	0.013	3.011	3.6	0.513	0.0245	0.0859	6.81	82	328	406	274	15	105	22	19	12	0	2	0.47
38	3	55	354.55	354.55*	0.41	3.01	6.57	21.9	0.018	0.016	2.676	7.1	0.443	0.0206	0.0772	5.36	76	292	333	282	16	384	23	20	12	0	3	0.55
38	3	85	354.85	354.85*	0.64	2.92	6.56	23	0.078	0.019	2.586	5.9	0.536	0.0195	0.0581	5.97	79	264	385	281	16	525	128	30	12	0	3	0.82
38	3	115	355.15	355.15*	0.58	3.14	7.57	25.1	0.012	0.013	3.048	3.4	0.523	0.0251	0.1324	6.51	81	311	343	279	15	135	410	15	12	0	2	0.49
38	3	145	355.45	355.45*	0.52	2.76	5.91	20.4	0.072	0.018	2.292	9.6	0.456	0.0166	0.1883	5.22	77	258	352	266	16	692	24	15	12	0	3	0.73
38	4	25	355.75	355.75*	0.55	3.42	7.67	25.3	0.034	0.012	3.054	2.7	0.529	0.0246	0.0913	7.21	83	320	319	292	15	109	22	14	12	0	2	0.53
38	4	55	356.05	356.05*	0.63	3.28	7.41	24.9	0.036	0.013	2.91	3.2	0.555	0.0239	0.1034	7.34	85	298	329	293	15	204	22	17	12	0	3	0.63
38	4	85	356.35	356.35*	0.56	3.49	8.07	26.6	0.024	0.012	3.169	1.3	0.577	0.0259	0.0632	7.52	86	334	318	299	15	26	21	18	12	0	2	0.5
38	4	115	356.65	356.65*	0.55	3.26	7.8	25.6	0.015	0.024	3.142	2.7	0.529	0.026	0.0635	6.48	81	318	459	290	15	67	80	29	12	0	2	0.46
38	4	145	356.95	356.95*	0.64	3.43	7.39	25.9	0.017	0.013	2.773	2.7	0.529	0.0286	0.0613	6.52	80	322	302	281	15	87	22	17	12	0	2	0.5
38	5	25	357.25	357.25*	0.53	3.15	7.57	24.9	0.018	0.027	2.912	3.9	0.519	0.0248	0.0615	5.56	76	302	404	289	15	88	62	15	12	0	3	0.53
38	5	55	357.55	357.55*	0.56	4.23	7.01	26.2	0.022	0.028	2.649	2	0.559	0.0277	0.0689	5.95	75	307	526	282	15	102	22	18	12	0	2	0.89
38	5	85	357.85	357.85*	0.56	3.38	7.71	25.9	0.021	0.028	3.042	2.3	0.533	0.0258	0.0573	6.82	84	354	304	293	15	50	22	15	12	0	2	0.58
38	5	115	358.15	358.15*	0.6	3.52	7.92	26.4	0.033	0.017	3.149	1.6	0.558	0.0259	0.0599	7.41	84	344	324	299	15	43	21	14	12	0	2	0.71
38	6	25	358.75	358.65*	0.48	3.32	7.56	24.7	0.023	0.032	3.126	3.6	0.502	0.0238	0.0968	7.07	81	321	306	274	15	124	22	15	12	0	2	0.59
38	6	55	359.05	358.95*	0.88	2.27	5.47	26.8	0.055	0.027	1.777	5.6	0.496	0.0195	0.0481	3.66	62	220	266	221	15	128	169	15	12	0	3	0.45
38	6	87	359.37	359.27*		1.5	2.55	9.1	0.107	0.023	0.964	25.8	0.173	0.0062	0.5715	1.8	58	166	311	176	17	1374	29	24	14	0	3	0.7
38	6	115	359.65	359.55*	0.51	2.9	6.27	23.3	0.029	0.017	2.371	6.7	0.478	0.0215	0.0886	5.11	70	278	328	266	15	417	84	24	12	0	3	0.53
38	6	145	359.95	359.85*	0.56	2.92	6.57	23.9	0.026	0.023	2.566	5.6	0.476	0.0199	0.069	5.48	72	267	317	269	15	365	118	16	12	0	3	0.52
38	7	25	360.25	360.15*	0.61	3.39	7.24	23.9	0.019	0.087	2.972	4.6	0.478	0.022	0.0925	5.86	79	315	320	273	15	155	23	14	12	0	3	0.5
38	CC	23	360.5	360.4 *	0.64	3.35	7.21	23.9	0.02	0.07	2.96	4.7	0.476	0.022	0.0885	5.84	74	279	324	270	15	158	22	17	12	0	3	0.47
40	1	6	370.46	370.46*	0.53	3.02	7.2	24.3	0.033	0.061	2.637	5	0.507	0.0236	0.0885	5.52	72	269	318	260	15	104	339	29	12	0	3	0.44
40	1	31	370.71	370.71*	0.49	3.27	7.45	23.8	0.032	0.041	2.792	4.6	0.517	0.0252	0.0965	5.97	75	305	311	267	15	94	430	21	12	0	3	0.48
40	3	51	373.91	373.81*	0.46	3.41	7.68	23.5	0.032	0.049	2.902	4.4	0.517	0.0257	0.1071	6.35	76	316	320	272	15	95	286	21	12	0	3	0.5
40	CC	31	376.9	376.45*	0.54	3.15	7.25	24.4	0.023	0.066	2.667	4.9	0.509	0.0241	0.0956	5.55	70	278	310	254	15	109	126	18	12	0	3	0.47
43	2	31	401.21	401.21*	0.64	3.76	6.01	22.7	0.069	0.026	2.329	7.3	0.425	0.0227	0.1634	5.13	70	287	313	270	15	235	33	15	12	0	3	0.52
43	2	50	401.4	401.4 *	0.44	3.29	6.43	22	0.057	0.018	2.435	7.3	0.455	0.0208	0.1365	5.81	73	282	326	266	16	567	140	16	12	0	3	0.57
43	2	101	401.91	401.91*	0.64	3.53	7.02	24.4	0.035	0.047	2.74	4.1	0.517	0.0254	0.0808	6.77	77	281	905	276	15	229	22	23	12	0	3	0.54
43	2	146	402.36	402.36*	0.55	3.12	7.41	24.8	0.021	0.041	2.722	4.1	0.523	0.0241	0.0747	5.34	71	292	302	276	15	96	22	21	12	0	3	0.5
43	3	41	402.81	402.81*	0.92	2.13	5.37	27.4	0.073	0.041	1.591	5.3	0.566	0.0233	0.0419	3.38	60	215	249	217	15	121	53	18	12	0	3	0.46
43	3	91	403.31	403.31*	0.72	3.69	7.64	26.4	0.052	0.126	2.845	1.6	0.588	0.0248	0.058	7.2	82	323	350	298	15	70	21	17	12	0	2	0.64
43	5	16	405.56	405.22*	0.61	3.31	7.2	24.9	0.038	0.045	2.618	4.2	0.55	0.0232	0.0604	5.58	70	274	472	285	15	210	22	21	12	0	3	0.59
Hole 731B																												
3	1	29	428.39	428.39*	0.73	3.6	4.72	23.5	0.086	0.295	1.316	7.6	0.478	0.0572	0.1786	3.99	61	238	260	189	15	176	65	25	12	0	3	0.64
3	1	60	428.7	428.7 *	0.48	3.28	7.06	23.7	0.083	0.039	2.513	5.7	0.497	0.0245	0.0803	5	68	289	304	263	15	153	53	19	12	0	3	0.48
3	CC	10	430.13	429.77*	0.78	2.87	5.61	25.5	0.035	0.09	1.743	5.3	0.445	0.0264	0.0406	3.75	60	248	259	209	15	139	23	21	12	0	3	0.58
5	1	51	447.91	447.91*	0.55	3.24	7.48	24.3	0.029	0.026	2.698	4.5	0.508	0.0242	0.0794	5.77	71	285	298	265	15	103	267	29	12	0	3	0.51
5	1	71	448.11	448.11*	0.53	3.11	7.34	24.1	0.034	0.03	2.655	4.9	0.49	0.0229	0.0904	5.65	70	261	306	257	15	78	309	24	12	0	3	0.6
Hole 731C																												
12	1	89	792.39	792.39*	0.87	2.31	5.28	25.6	0.034	0.026	1.578	5	0.408	0.0204	0.0359	4.23	60	169	254	194	15	118	23	24	12	0	3	0.68
12	2	90	793.9	793.55*	0.59	2.84	7.26	24.3	0.03	0.03	2.503	5.1	0.5	0.0218	0.0929	5.51	70	255	303	266	15	64	430	17	12	0	3	0.37
17	1	141	918.11	918.11*	0.84	2.4	5.78	25.7	0.03	0.024	1.897	4.6	0.411	0.017	0.037	4.37	61	175	250	212	15	89	423	17	12	0	3	0.57

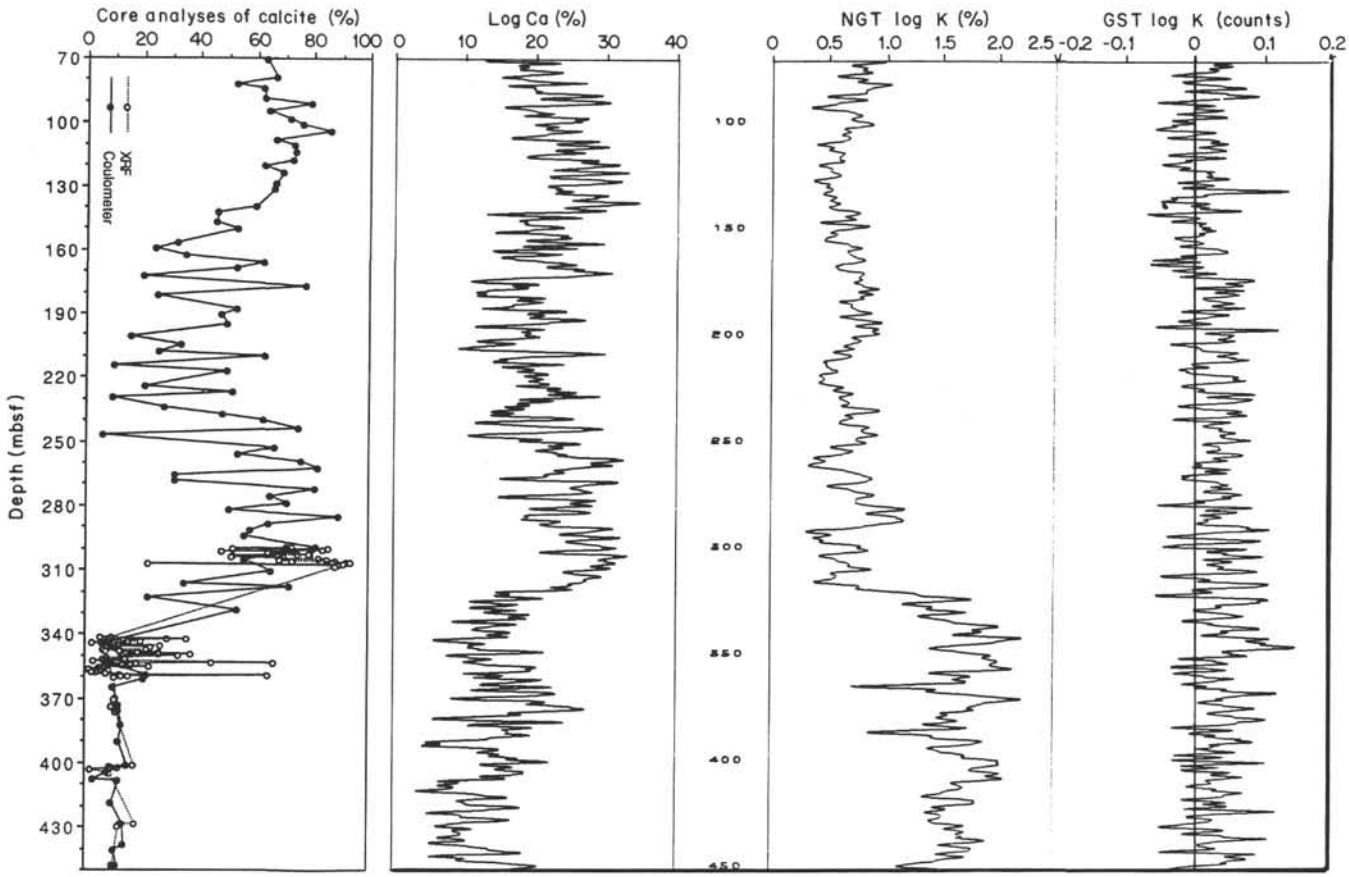

Figure 1. Comparisons among geochemical indicators at ODP Site 731, for 70–450 mbsf. Discrete core measurements of calcite percentage (Prell, Niitsuma, et al., 1989; this paper) confirm the overall accuracy of the calcium log; detailed comparison is not possible because of very different sampling volumes. The change from carbonates above 320 mbsf to terrigenous turbidites below 320 mbsf is evident on both the calcium and NGT potassium log. The GST potassium log (far right) appears to be unreliable.

The repartitioning of Cl and K has a significant but not overwhelming effect on the character of the other GST elements Ca, Si, Fe, Ti, and S (e.g., Fig. 2). This repartitioning is expected to slightly improve the reliability of the geochemical logs.

Following repartitioning, the yields of Ca, Si, Fe, Ti, S, and Gd were divided by (unfortunately proprietary) Schlumberger sensitivity coefficients, which convert from spectral yields to approximate elemental concentrations. For example, Gd yields are similar to those for Ti, because of the huge Gd capture cross section; the sensitivity coefficients reduce the apparent Gd concentrations to ppm and Ti concentrations to 0%–1%. Occasional negative concentrations are truncated at zero; except for Ti and S yields, this truncation was rarely needed. Finally, elemental concentrations were normalized by dividing by the sum of the oxide concentration. For this final step, K and Al oxides were included when available. For Sites 728 and 731 at which Al was not logged, an Al/Ti ratio of 11.6 was used in this step; its effect on the character of resulting element logs is minor.

The log processing steps described above differ from the normal geochemical processing, in order to maximize the reliability obtainable independently of any XRF information. This difference decreases the direct applicability of our subsequent log/XRF comparison to other ODP holes at which "normal" processing was utilized. However, a processing procedure similar to ours could be used on the other holes as well, if a similar type of analysis shows that it is appropriate.

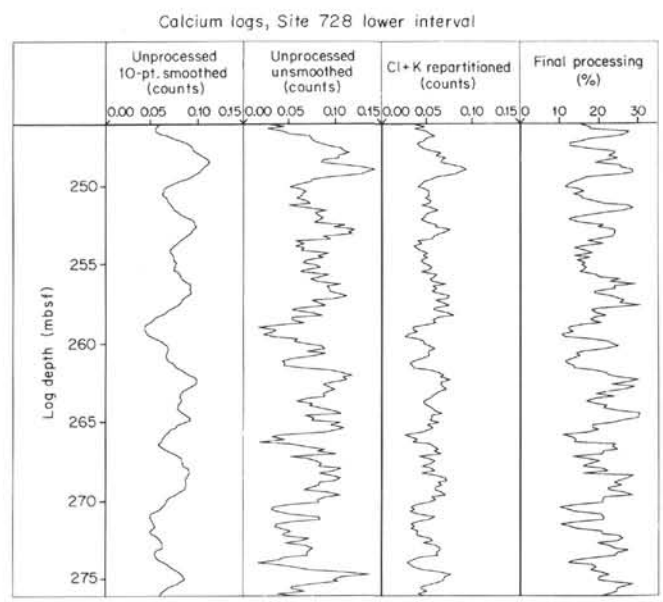

Figure 2. Effect of processing technique on the character of the calcium log. The leftmost curve is the normal processing employed for GST data; the rightmost curve is the final processing used here for comparison to XRF data.

COMPARISON OF XRF TO LOGS AS A FUNCTION OF DEPTH

High-resolution sampling for XRF was undertaken for seven depth intervals, varying from 5 to 30 m in length. Three intervals were sampled at Site 723; two intervals were sampled at both Site 728 and Site 731. The number of XRF samples per interval (Table 4) varies dramatically, from a minimum of 18 samples in interval 4 to 123 samples in interval 5. Figures 3–9 show overlays of log and XRF measurements as a function of depth for each of the seven intervals, for each of the elements Ca, Si, K, Ti, Fe, S, and Al.

The focus of these comparisons is on the character of geochemical variations as a function of depth, not on the absolute magnitudes of log-based elemental abundance in comparison to XRF-based abundance. Except perhaps for K and Al (which are reputed to be directly determined in volume percent), we do not expect our processing procedure to have accurately estimated concentrations. For example, by repartitioning all K counts rather than using the NGT to predict an average K count and repartitioning the residual from this average, we have effectively imparted a baseline rise in estimated abundances of Ca, Si, S, and Gd and a drop in estimated abundances of Ti and Fe. In the last portion of this section, we briefly examine the consistency of log and XRF magnitudes.

Depth uncertainty is the major limitation to almost any comparison of log and core data. Ship heave causes some uncertainty in both core and log depths; fortunately, seas were extremely calm during coring and logging of Sites 723, 728, and 731. Drill pipe stretch and particularly logging-cable stretch cause further mismatch; this mismatch is reduced by adjusting all initial log depths to a pipe standard, based on the log response to the base of pipe. Further correction for cable stretch can be accomplished by depth-shifting an entire log, based on matching similar features in logs and cores. For the comparisons of log and XRF abundance variations shown in Figures 3–9 and considered subsequently, we have depth-shifted all logs with respect to the core XRF data by a constant amount within each interval (Table 4). This slight depth shift (average 1.6 m, maximum 3.8 m) is based on matching of apparently correlative portions of XRF and log Ca peaks. Shift estimates are more similar for different intervals within a site than between sites, as expected because differential cable stretch is much less over short intervals than between holes with different water depths.

Incomplete core recovery is probably the biggest source of depth mismatch. Even with XRF sampling confined to highest recovery intervals, depth shifts of a meter or sometimes more are expected. Susceptibility correlations between overlapping piston cores show that "100%" recovery cores are actually missing the top 10–30 cm of material (P. deMenocal, pers. comm.); apparently the piston coring process causes some core stretching. No comparable analysis of XCB cores has been undertaken. The ODP recording convention is to "hang" cores from the top of their cored interval, thereby assuming that any missing material was lost from the bottom of the cored interval. As previously discussed, this procedure seems particularly appropriate for Site 723. Yet a comparison of XRF and log Ca concentrations for the middle interval from Site 723 (Fig. 10) shows that this assumption is only a good first approximation. Because of the high-resolution character of the XRF and log measurements, one can see that the top core in this interval needs to be shifted upward, indicating that the missing material comes from the top of the core rather than from the bottom. This interval is the only one in which a differential shift of XRF data was applied within an interval. Similar but perhaps smaller differential shifts are certainly present within the other six intervals; none were applied because the evidence was less compelling. Nevertheless, when visually comparing the character of XRF and log elemental-abundance variations on any of the plots of Figures 3–9, one must keep in mind that slight depth mismatches between peaks may or may not be caused by core recovery problems.

Table 4. Intervals with high-density XRF sampling.

Interval no.	Hole	Core depths (mbsf)	Number of XRD samples	Lithology
1	723B	92.74–102.85	30	Clayey carbonate
2	723B	208.65–233.68	93	Clayey carbonate
3	723B	381.25–386.10	18	Clayey carbonate
4	728B	178.55–182.80	18	Clayey carbonate
5	728B	247.75–277.35	122	Clayey carbonate
6	731A	299.53–308.50	30	Carbonate ooze
7	731A	341.60–360.15	59	Silty clay

Our comparison is less hampered by the depth-shift problem than are some studies which relied on widely-spaced XRF measurements, because the high-resolution XRF character allows some refinement of depths. However, the best known comparison—the Conoco test well (Chapman et al., 1987)—was even less affected by depth shifts, because the stratigraphy there is characterized by several thick and relatively uniform-mineralogy beds, rather than our rapidly varying lithologies.

One further complication to a comparison of XRF and log geochemistry is the much different measurement volumes of the two methods. Our XRF measurement volumes were 10 cm^3. In contrast, the geochemical tools average a volume of about 1 m^3 and have a vertical averaging distance of about 0.5 m. ODP GST logs routinely have a 10-point (1.52 m) averaging applied for suppression of random noise, and the NGT logs use a variable-length (but generally shorter) Kalman filter. Intervals such as 4 and 5 exhibit a strong cyclicity with a wavelength of only about 2 m, based on visual core descriptions, susceptibility core logging (Prell, Niitsuma, et al., 1989), and our XRF data. A 1.5 m smoothing is clearly too long for such intervals and seriously obscures detection of the major geochemical variability. Consequently, we use only a 3-point (0.45 m) log smoothing in Figures 3–9 and no smoothing at all in subsequent principal components analysis. The very mild log smoothing, high-resolution (0.25–0.30 m) XRF sampling, and gradual (m) lithologic changes in the cores result in minimal problems of incompatible vertical resolutions between cores and logs. Examination of Figures 3–9 shows that almost all XRF peaks and troughs are defined by several adjacent XRF measurements rather than by a single measurement, so that these peaks and troughs are at least theoretically resolvable by the logs.

In the remainder of this section, we consider the comparison of XRF data with geochemical logs on an element-by-element basis. The largest lithologic change within the three sites is the downhole change from nannofossil ooze to terrigenous turbidites at Site 731. We begin discussion of each element with an examination of whether the geochemical logs reliably detect this major change. We then discuss the extent to which the logs have reproduced the small-scale variability within each of the seven intervals of Figures 3–9 and Table 4.

The primary criterion for this comparison is qualitative character match of this small-scale variability. In general, we neither expect nor obtain similar means or similar ranges of concentrations between XRF and geochemical logs, because proper scaling of the logs to elemental percentages is not possible unless all major elements are determined. However, Figures 3–8 are not scaled to facilitate character match; instead they have identical vertical scales for log and core data to optimize comparisons of means and standard deviations. A secondary and more quanti-

tative comparison within each interval is the correlation coefficient. For calculation of the correlation coefficient, the reprocessed but unsmoothed element logs were resampled at the same depths as the XRF measurements. We omitted the first four XRF measurements from interval 1 and the first three XRF measurements from interval 3. XRF sampling for interval 1 was originally thought to have begun exactly at the start of openhole geochemical logging; however, the subseqently determined 1.2 m depth shift between the two data sets means that no openhole logs are available at the top of interval 1. The element logs at the very top of interval 3 exhibit excursions to bizarre concentrations, caused by negative silicon yields which exaggerate excursions of all elements during the oxide normalization step. These obviously unreliable data are omitted in the statistical evaluation of the remainder of interval 3.

Calcium

Calcium is the only element for which a substantial core-based dataset exists in addition to our XRF data. Shipboard measurements of calcium carbonate percentage were made by coulometer at approximately 5–10 m intervals throughout Sites 723 and 728 and in the upper half of Site 731. The Site 723 and 728 carbonate data are of little value for our purposes, because both logs and XRF indicate that the vast majority of the carbonate variance resides in wavelengths of less than 5 m. However, broad variations in carbonate are seen in the coulometer results from Site 731.

Figure 1 plots both the 87 coulometer measurements and 106 XRF measurements of carbonate for the interval 70–450 mbsf; 70 mbsf is just below the base of pipe for geochemical logging, and 450 mbsf is the change from continuous coring to spot coring. The Ca log for this interval (Fig. 1) exhibits a reasonable agreement with the core data. The base of the carbonates, at 320 mbsf, is obvious in both log and core data. The wide variability of discrete coulometer measurements makes this boundary appear more gradual in core than in log data. Visual core descriptions (Prell, Niitsuma, et al., 1989) also suggest a gradual transition, but other logs (e.g., velocity and neutron porosity) confirm that a sharp lithologic change occurs at 320 mbsf, with a continuing and more gradual transition below that depth. Within the carbonates, the logs and cores indicate that the intervals 70–140 mbsf and 240–315 mbsf have the highest carbonate content. In the intervening interval 140–240 mbsf, visual core descriptions indicate numerous beds of diatomaceous mud and a general dilution of the nannofossil ooze carbonate by diatoms. As a result, both the log and coulometer calcium records exhibit very high variability and generally lower calcium than in adjacent depth intervals.

Both the log Ca and core carbonate data indicate that the lowest average $CaCO_3$ is in the turbidites, below 320 mbsf. However, the Ca log shows values for 350–405 mbsf that—though quite variable—are almost as high as 140–240 mbsf; in contrast, the core carbonate data are only rarely as low in the interval 140–240 mbsf as in the turbidites. The raw, unreprocessed Ca log (Prell, Niitsuma, et al., 19S9) is more consistent with core data in this respect; it is consistently lower in the turbidites than in the diatom-rich carbonates of 140–240 mbsf. This baseline difference between raw and reprocessed Ca logs is probably attributable to our arbitrary choice of a chlorine baseline for the chlorine repartitioning. The upper turbidites had perhaps the greatest variation in hole diameter of any sediments logged on Leg 117. Consequently, this interval is subject to major uncertainty concerning the relative proportions of the Cl small-scale variability that are due to hole size and partitioning problems. Normally, a caliper log would help to resolve this question, but no reliable caliper was obtained at Site 731. Indeed, none has been available to ODP until Leg 125.

Of the two Site 731 intervals with high-resolution XRF sampling, the upper interval (interval 6 of Table 4) is in nannofossil ooze and the lower interval (interval 7) is in the low-carbonate terrigenous turbidites. The ratio of mean Ca concentration for the lower interval to that of the upper interval is 0.22. For comparison, the Ca log yields a ratio of 0.43. Clearly, the Ca log readily detects the major difference in Ca concentration between these two intervals. The difference in ratios is probably attributable to the overestimation of the relative amount of Ca in the turbidites.

The results from the Conoco test well indicated a Ca precision of 2% (Chapman et al., 19S7). As previously discussed, ODP geochemical logging precision might be expected to be less than at the Conoco test well. Six of our seven intervals have a standard deviation of XRF Ca concentrations of more than 2% (Table 5). Thus we might anticipate that the general character of XRF Ca variations would be detectable by the Ca log. Figure 3 compares the two data types for the seven depth intervals. Qualitatively, the character match between core and log Ca variations ranges from fair to very good (Table 5).

The correlation coefficient (R) between the two data types is a more quantitative comparison. However, R is severely degraded by any residual depth shifts. Longer depth intervals are more likely to contain differential depth shifts within the XRF data due to incomplete core recovery. As a result, the longer depth intervals generally have lower R (Table 5), particularly for our best determined log: Ca. In particular, the longest interval (interval 5) shows a very good match of XRF and log Ca below 257 mbsf but a poor match above this depth (Fig. 3). The resulting correlation coefficient is only 0.17. A residual depth shift of about 1 m for the XRF data above 257 mbsf would substantially improve the match. We note that 257 mbsf occurs within a core with nominal 101% recovery and with some core disturbance, but we do not feel that the character match between XRF and logs above 257 mbsf is sufficient to confidently infer that a shift is present.

Based on the correlation coefficient between XRF and log Ca, intervals 1–4 strongly confirm the ability of the Ca log to reliably detect Ca variations of 2%–7%. The correlation coefficient calculations of Table 5 exclude the first three XRF measurements of interval 3; the previously discussed log normalization problem at these depths yields absurdly high log Ca values there (Fig. 3). Intervals 4 and 7 exhibit a good character match, but gradual drift in the Ca log baseline is evident as a gradual downhole increase in Ca values that is not confirmed by the XRF data. A single very low-Ca XRF point in interval 6 is not detected by the log. This anomalous point is evident on plots of other elements as well (Figs. 4–9) without a corresponding log response, and we suspect that it is a very thin bed below the resolving power of the logs.

Based on these comparisons of Ca logs with both coulometer measurements of $CaCO_3$ and XRF measurements of Ca, we conclude that the Ca log does detect Ca variations larger than about 2%. However, some residual repartioning problem can cause drift of the Ca log. We suspect that partitioning between Cl and Ca yields is the problem, and we think that further processing tests on these or other geochemical logs are warranted.

Silicon

The change from nannofossil ooze in interval 6 to terrigenous turbidites in interval 7 causes an increase in average silicon abundance from 7% to 23% (Table 5). This increase is much larger than the estimated Si log precision of 1.5% (Chapman et al., 1987) and should be quite evident on the Si log. The Si log exhibits a factor of 2.1 increase, quite significant but less than the factor of 3.2 increase in XRF Si abundance.

Table 5. XRF elemental results by interval. Both subjective (fit) and objective (correlation coefficient R) matches to logs are shown.

Top depth		92.74	208.65	381.25	178.55	247.75	299.53	341.60
End depth		102.85	233.68	386.10	182.80	277.35	308.50	360.15
Number		30	93	17	18	122	30	59
Ca	Mean	20.5	22.0	20.0	21.4	21.5	29.3	6.6
	σ	1.6	2.6	7.3	3.3	3.9	6.2	5.2
	fit	G	VG	F	VG	G	F	G
	R	0.47	0.61	0.72	0.56	0.17	0.23	0.26
Si	Mean	11.6	9.9	12.2	10.9	11.6	7.0	22.7
	σ	1.2	2.5	6.0	2.2	2.5	4.1	3.9
	fit	F	G	P	G	F	F	F
	R	0.54	0.49	0.33	0.27	0.04	0.14	0.32
K	Mean	0.89	0.74	0.71	0.76	0.79	0.78	2.55
	σ	0.21	0.35	0.84	0.51	0.58	0.90	1.24
	fit	F	F	G	G	F	F	P
	R	0.26	0.14	0.08	0.37	0.14	−0.21	−0.05
Ti	Mean	0.27	0.21	0.21	0.21	0.22	0.13	0.47
	σ	0.03	0.04	0.09	0.05	0.06	0.08	0.09
	fit	P	F	F	G	F	P	P
	R	−0.01	0.09	0.64	0.46	0.11	0.06	−0.05
Fe	Mean	1.91	1.77	1.82	1.91	1.93	1.42	5.74
	σ	0.08	0.16	0.29	0.18	0.22	0.44	0.50
	fit	F	P	P	F	F	G	P
	R	0.04	−0.19	0.23	0.48	−0.04	0.28	−0.37
S	Mean	0.59	0.84	1.22	0.61	0.47	0.018	0.020
	σ	0.10	0.16	0.29	0.09	0.11	0.006	0.011
	fit	P	P	G	G	F	?	?
	R	0.48	0.02	0.69	0.33	0.12	0.28	0.27
Al	Mean	2.74	2.27	2.21				
	σ	0.23	0.48	0.87				
	fit	F	G	F				
	R	0.18	0.56	0.55				

Based on XRF, six of the seven intervals of Table 5 have standard deviations of Si abundance greater than 1.5%. Thus one anticipates that the Si log should be able to capture much of the small-scale variability detected by XRF in these intervals. The qualitative match between XRF and log Si character in these intervals (Fig. 4) ranges from fair to good. Correlation coefficients are moderately good, with the exceptions of intervals 5 and 6. Interval 5 does not exhibit a very convincing match between XRF and log Si, even below the previously discussed zone with a possible depth-shift problem. Intervals 2, 6, and 7 show several Si log drops to near zero that are inconsistent with the XRF results; these excursions are probably indicative of a partitioning problem in the inversion of GST spectra. In summary, Figure 4 shows that core silicon variations of 2%–6% are often but not consistently detected by the Si log.

Potassium

The change in potassium content at the base of the carbonates at Site 731 is clearly detectable in the NGT potassium log (Fig. 1). The mean XRF K content for the lower XRF interval at this site is 3.3 times that for the upper interval. The corresponding K log intervals give a ratio of 2.6, demonstrating that this major change in K is recorded by the log with reasonable fidelity.

Six of the seven intervals of Figure 5 have a higher standard deviation of XRF-based K than the nominal 0.25% precision cited by Chapman et al. (1987). Thus one might anticipate a relatively good match of XRF and log small-scale character for K. However, the character match ranges from poor to good and is mostly only fair (Fig. 5). Correlation coefficients (Table 5) are generally low and positive, with the poorest fit occurring in interval 7, which has an XRF standard deviation 5 times the nominal resolution limit. We suspect that the poor K log for interval 7 results from borehole effect. This interval has wide swings in borehole diameter due to washouts, but we are unable to apply the normal hole-size corrections to the NGT logs because no reliable caliper was obtained on Leg 117.

Intervals 1–3, from Site 723, exhibit only a fair visual match of K log to XRF K; correlation coefficients are also low. Further, replicate NGT logging passes had only a fair agreement. In contrast, replicate uranium logs obtained simultaneously by the NGT showed very good agreement and the highest U concentrations that we have seen (Prell, Niitsuma, et al., 1989). Apparently the anomalously high U, associated with extremely high concentrations of organic matter at this site, exaggerates slight problems in the inversion of the natural gamma spectrum for K, Th, and U. This possible inversion problem, coupled with a K variation only slightly higher than the nominal resolution of the NGT, results in the low-quality match with XRF.

Interval 6 has a visually good match of log K with XRF with an indication of a slight, half-meter depth shift between cores and logs; this depth shift is sufficient to degrade the correlation coeffient to a negative value. The K log from interval 7 is the only element log from this interval that shows some evidence of partly detecting the very thin bed represented by one XRF sample (Fig. 5). However, the K logs of Figure 5 generally have lower vertical resolution than the GST element logs of Figures 3, 4, 6, and 7, because of the variable-length Kalman filter applied by Schlumberger processing. For example, the 2-m cyclicity of interval 5 appears to be only marginally resolved by the K log.

The surprisingly low quality of our K log match with XRF indicates a strong need for further evaluation of NGT K logs, on wells with either a relatively uniform hole size (e.g., basalt) or a reliable caliper log of hole size.

Titanium

The transition from carbonates to turbidites at Site 731 causes an increase in XRF titanium by a factor of 3.6. The Ti log gives a much lower ratio of 2.0, but this difference is not surprising because the XRF-based difference is only 0.3%, compared to a nominal 0.1% resolution of Ti logs (Chapman et al., 1987).

All seven intervals of Figure 6 are lower to much lower in XRF Ti than the nominal 0.1% resolution, so little to no match

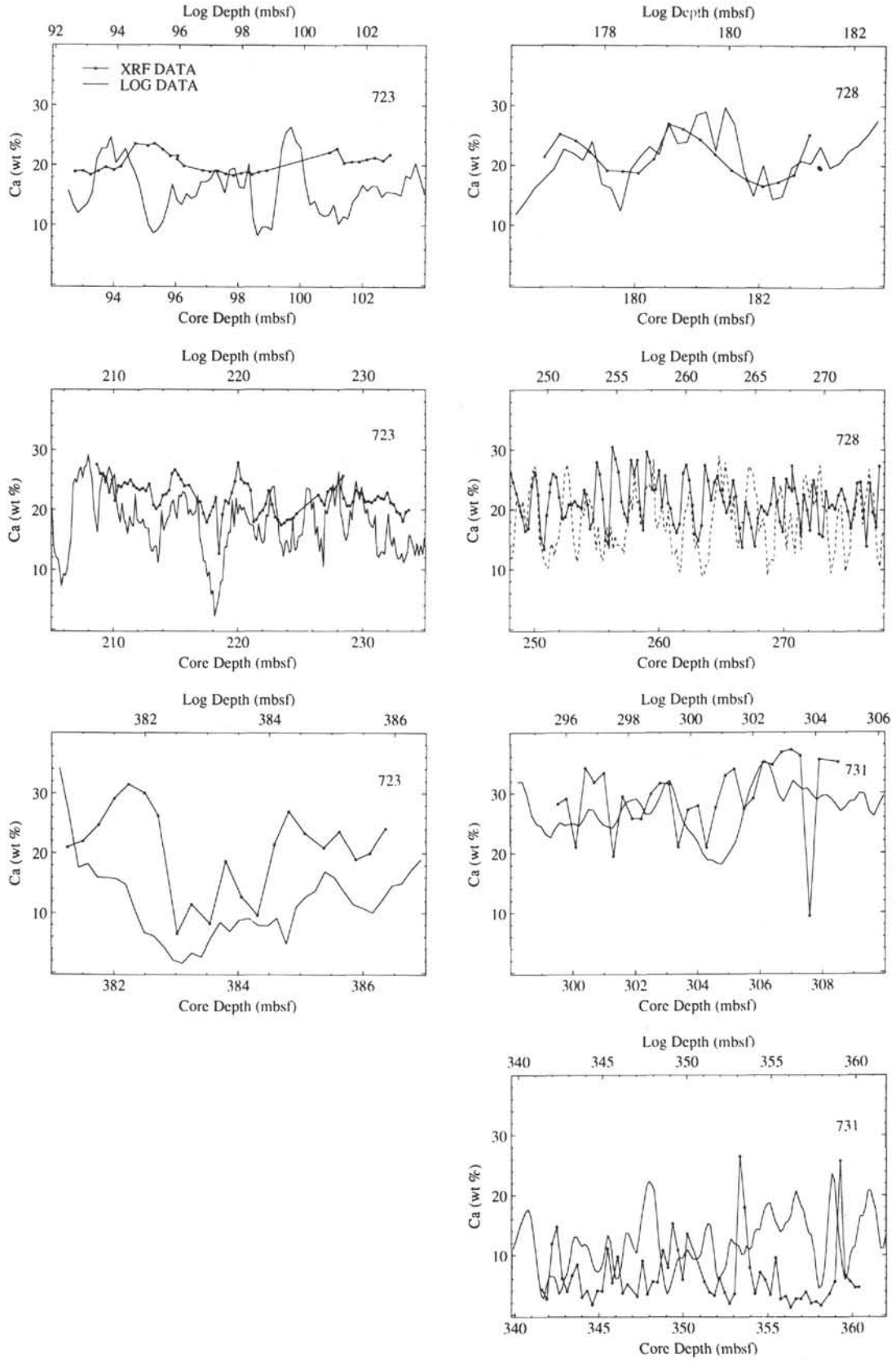

Figure 3. Comparison of XRF and geochemical log determinations of calcium, for the seven intervals of Table 1. Log data are indicated by solid or dashed lines with no symbols. Solid squares connected by solid lines indicate XRF data. The focus here is on the extent to which the character of the two data types agrees, not on absolute percentages.

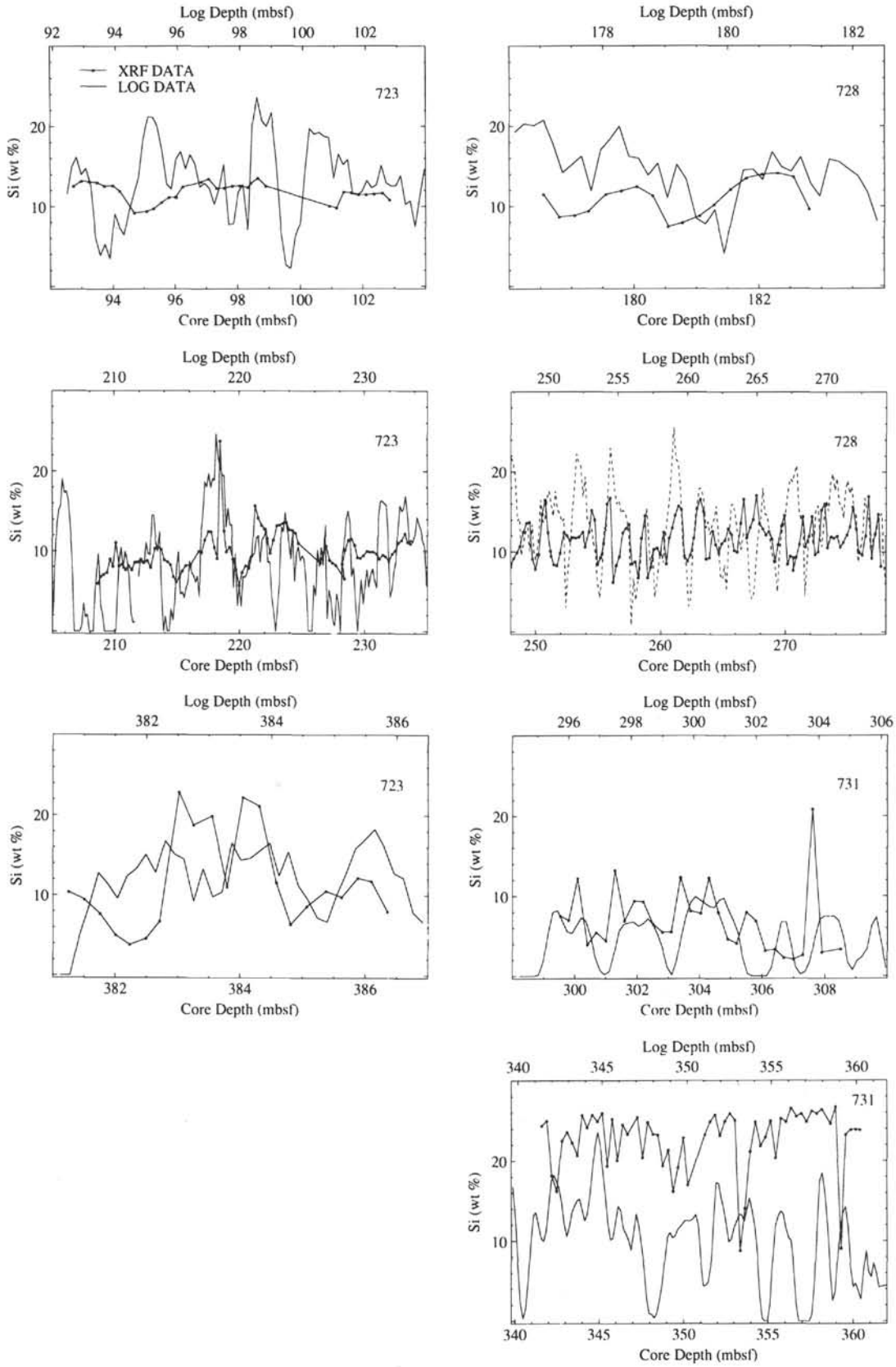

Figure 4. Comparison of XRF and geochemical log determinations of silicon, for the seven intervals of Table 1. See Figure 3 for explanation.

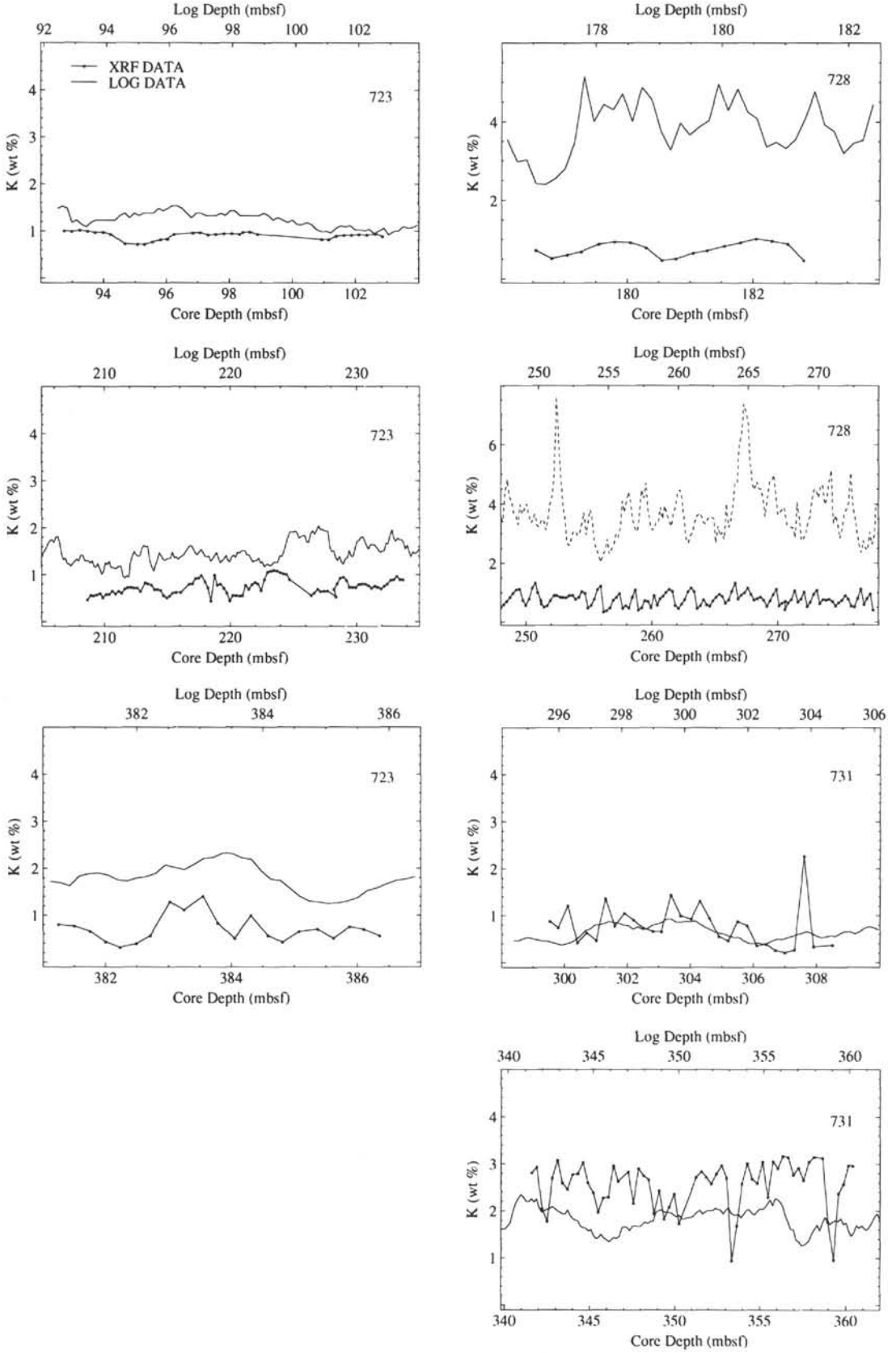

Figure 5. Comparison of XRF and geochemical log determinations of potassium, for the seven intervals of Table 1. See Figure 3 for explanation.

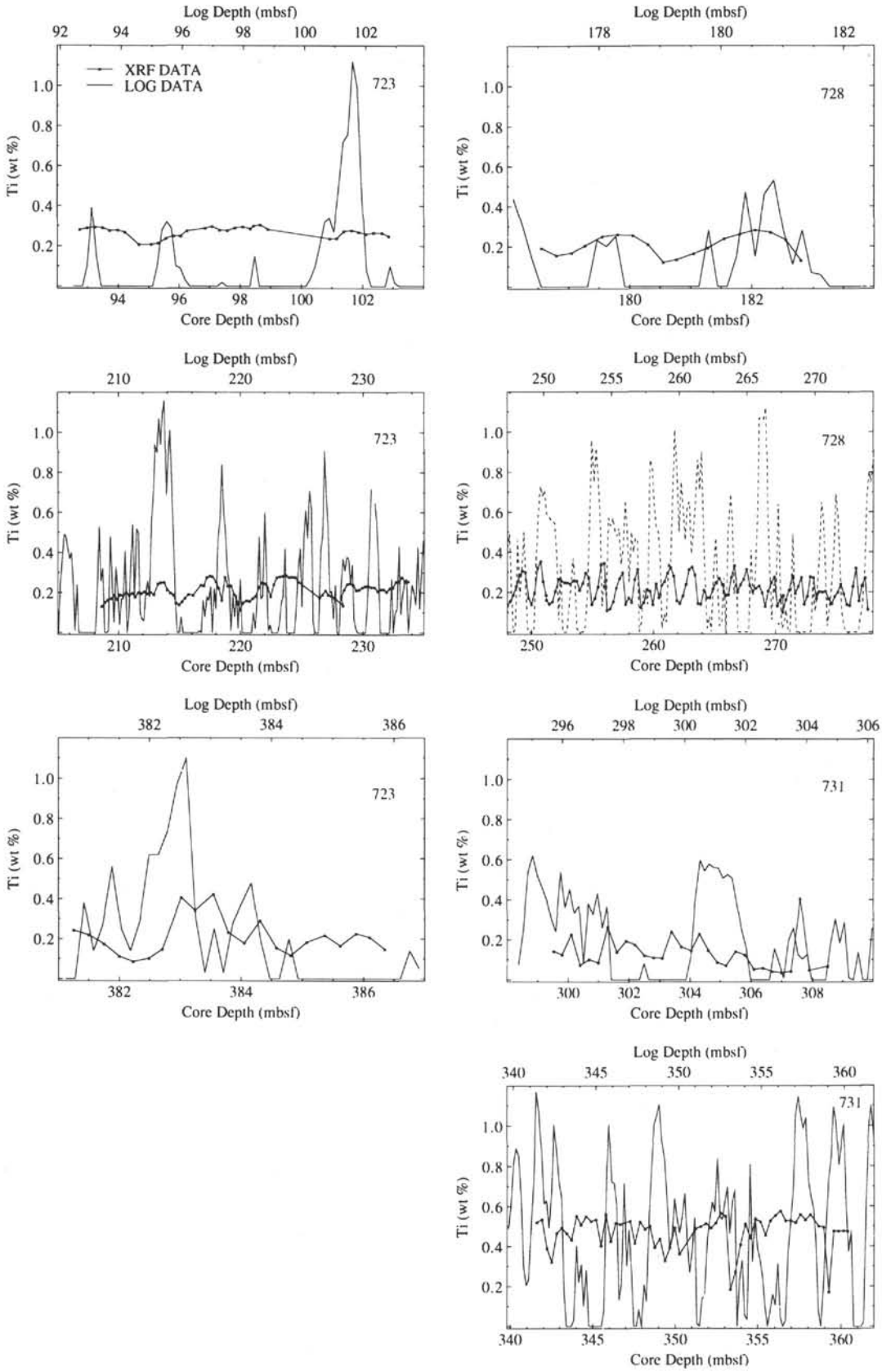

Figure 6. Comparison of XRF and geochemical log determinations of titanium, for the seven intervals of Table 1. See Figure 3 for explanation.

of log to XRF is anticipated. The actual match is mostly poor-fair, with near-zero correlation coefficients. Exceptions are intervals 3 and 4, with good visual matches and high correlation coefficients of 0.5–0.6, though the XRF-based variation in Ti is no higher in these intervals than in interval 7, where the match is only poor.

Titanium counts after Cl and K repartitioning often go negative; these negative counts are truncated at zero in Figure 6. The repartitioning of all K that we employed lowered Ti counts too much, by effectively assuming that true K concentration is zero. The normal Schlumberger processing, which uses the NGT K log to estimate the amount of GST K to be repartitioned, probably would have resulted in a more reliable Ti log. However, the unusually low accuracy of our NGT K log might have limited this improvement, even if we had the complete geochemical suite of logs required for this type of processing. We conclude that geochemical logging has promise for detecting Ti variations of $<0.1\%$, if partitioning interference with K (and possibly S) can be reduced with a reliable NGT K log. Stacking of replicate NGT runs might accomplish part of this needed NGT improvement; a reliable caliper for borehole correction probably would help even more.

Iron

The transition from carbonates to turbidites at Site 731 causes an increase in XRF iron by a factor of 4.0. The Fe log increases by a factor of only 1.6 over the same intervals. The major change is thus reliably detected in a qualitative sense, but an Fe calibration problem is suggested.

Within the two intervals of Site 731 (intervals 6 and 7), the variation observed in XRF measurements of Fe is about the same as the nominal Fe resolution of 0.5% (Chapman et al., 19S7) and the variations are expected to be marginally resolvable by the log. In contrast, intervals 1–5 (Sites 723 and 728) have much lower XRF Fe variability than 0.5% and are not expected to be resolvable. The qualitative match between XRF and log Fe is poor to fair (Fig. 7), with correlation coefficients low and as often negative as positive (Table 5). Exceptions are interval 6 with a good visual fit and $R = 0.28$ and interval 4 with a fair fit and $R = 0.48$. Thus the 0.5% resolution estimate of Chapman et al. (1987) appears to be reasonable for our ODP Fe logs.

Sulfur

The transition from carbonates to turbidites at Site 731 has no significant change in XRF sulfur content. Further, the XRF S at Site 731 is two orders of magnitude lower than the nominal 1.5% log resolution for sulfur of Chapman et al. (1987). Thus, unlike the case for the other elements, this transition is not useful as a test of S log reliability.

Intervals 1–7 all have XRF S variations that are 1–2 orders of magnitude lower than the nominal S log resolution. Thus it is unsurprising that intervals 1 and 2 have a poor character match of XRF and log S (Fig. 8), as well as zero to negative correlation coefficients (Table 5). It is surprising that intervals 3–5 have a fair to good character match, with fair to very good correlation coefficients (e.g., 0.69 for interval 3). This agreement may be an indication of poor partitioning rather than of unexpectedly very high resolving power of the S log. Intervals 1 and 2, with a poor match, have no XRF correlation between S and the noncarbonate elements, whereas intervals 3 and 4 with a good match do have a good XRF correlation between S and the noncarbonate elements. The sulfur concentrations from logs are much higher than the XRF sulfur concentrations, further suggesting a partitioning problem. Thus the "S log" may actually represent a poorly partitioned composite of at least one other non-carbonate element. However, a pilot repartitioning of all S to other elements for Site 728 yielded revised Si, Fe, Ti, and Ca logs that were almost identical to those of Figures 3, 4, 5, and 6; only the revised Ca log had any noticeable (but trivial) change in character.

Aluminum

Aluminum logging was undertaken only at Site 723. The XRF Al variations in intervals 2 and 3 (Table 5) are slightly less than the nominal 1% Al resolution of Chapman et al. (1987), while variations within interval 1 are much less than we can expect to resolve. The character match of XRF and log Al ranges from fair to very good among the three intervals; high correlation coefficients of 0.56 and 0.55 are found for intervals 2 and 3. These data suggest that Al character is useful for variations of $>0.2\%$–0.4%. However, our absolute accuracy is poor: both the mean Al and range of Al values based on logs are much too high in all three intervals of Site 723. Our absolute accuracy for Al is degraded by lack of a caliper and therefore of hole-size correction to the aluminum log.

Geochemical Log Accuracy

The element-by-element analyses above focus on the fidelity with which geochemical logs detect the character of geochemical variations within the formations. They do not consider accuracy, the extent to which the magnitudes of XRF abundances are duplicated by the geochemical logs. In a preceding section on geochemical log processing, we noted that the Leg 117 geochemical logs cannot be converted to weight percentages, because this conversion requires information on all major elements, obtainable only with both a log of photoelectric effect and the full suite of geochemical logs. Because many sites other than those on Leg 117 do not obtain all logs, a brief discussion is warranted of the accuracy resulting from the less reliable alternative processing utilized here. We focus on a comparison between logs and XRF of the average and within-interval variability for each element. Means and standard deviations could be used, but qualitative examination of Figures 3–9 is adequate.

Calcium concentrations (Figs. 3 and 10) appear to be estimated fairly well by our processing procedure. Both the average concentration and the intra-interval ranges of concentrations are generally comparable for logs and XRF. Exceptions are log variations that are too high in interval 1, concentrations that are too low in interval 3, and the previously-discussed too-high Ca concentrations of interval 7.

Average silicon concentrations (Fig. 4) from logs also agree with XRF. Notable exceptions are the drops to zero in intervals 2, 6, and 7, attributable to occasional partitioning problems. Also, silicon concentrations are too low in interval 7, because of the too-high Ca concentrations. The range of Si log variations within each interval is too high, particularly in interval 1 and whenever Si drops out to zero.

Potassium concentrations (Fig. 5) are too low in interval 6 and especially in interval 7, where variable and enlarged hole sizes degrade the reliability of the K log and introduce large, spurious variations in apparent K concentration. K concentrations are too high at Site 723, possibly a result of the NGT inversion problem introduced by anomalously high uranium at this site.

Titanium log variations (Fig. 6) are much too high, and log abundances swing between values that are much too high and dropouts to zero concentration. An identical problem is evident for sulfur (Fig. 8), which is actually present in concentrations so low that it should yield constant and near-zero GST counts in all intervals.

Iron concentrations in logs (Fig. 7) are much too high, by a factor of 1.5–4. The inter-element range of Fe is reasonable in most intervals (an exception is interval 1). A baseline shift is implied, but its source is unknown.

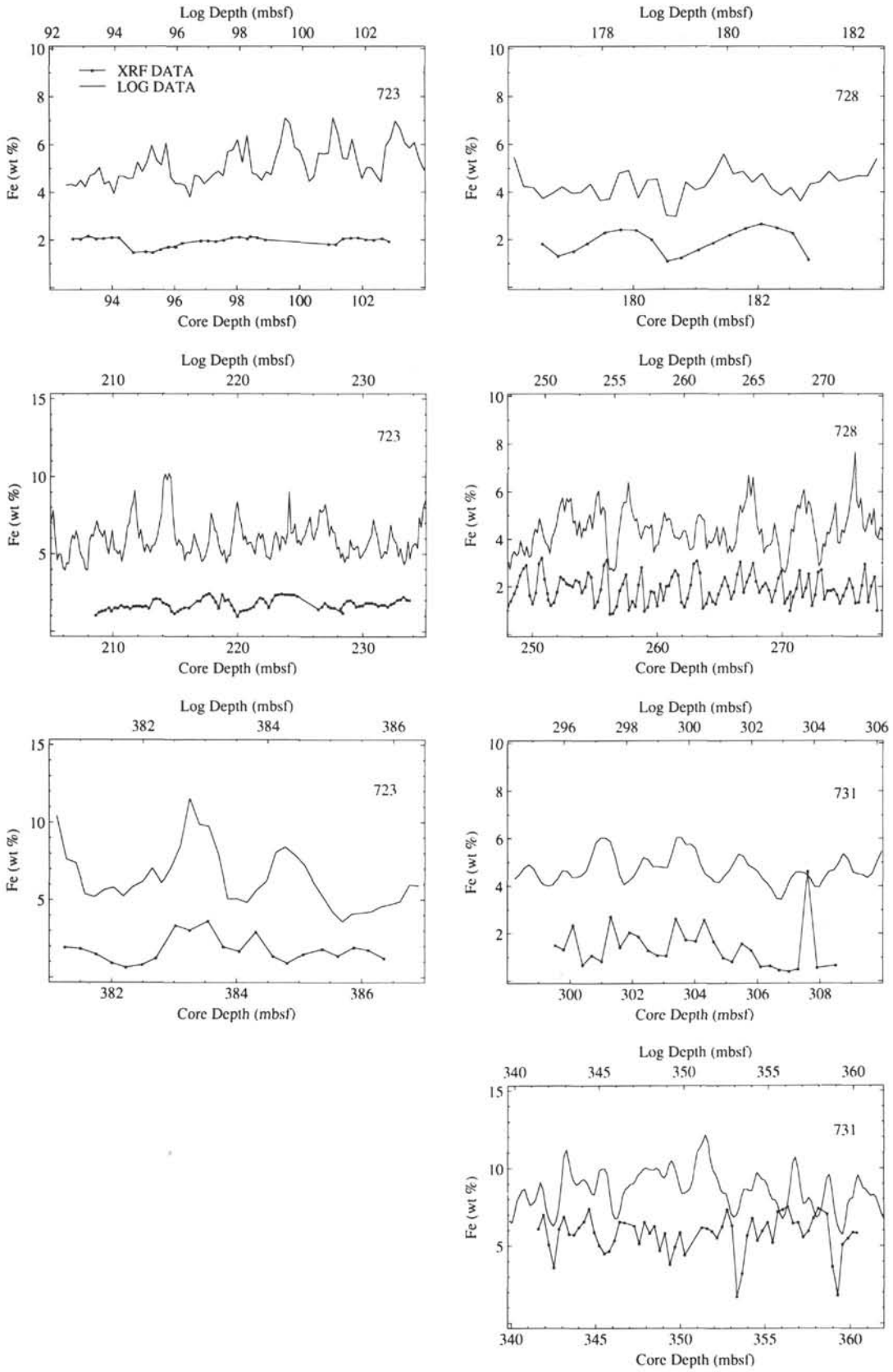

Figure 7. Comparison of XRF and geochemical log determinations of iron, for the seven intervals of Table 1. See Figure 3 for explanation.

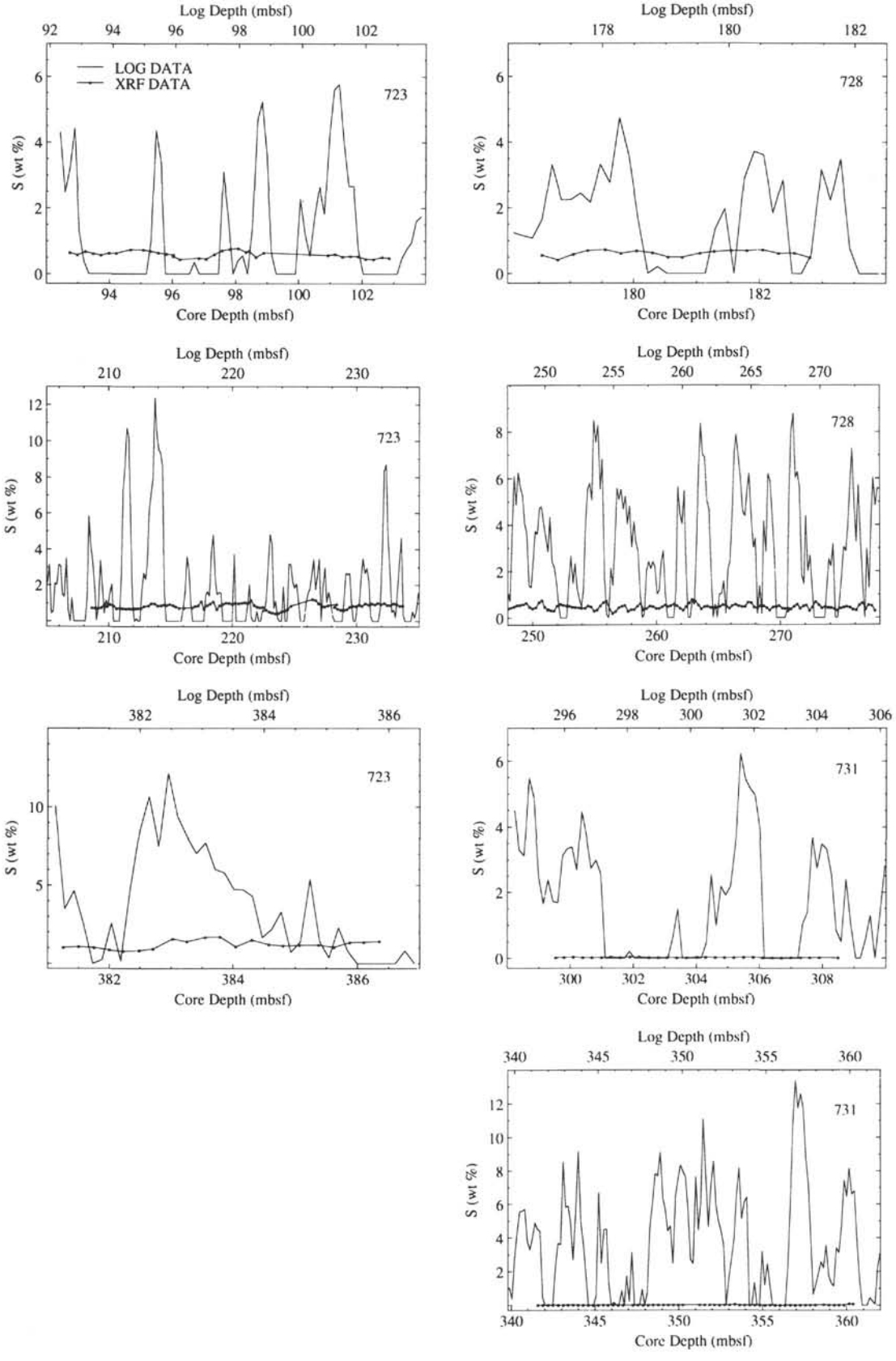

Figure 8. Comparison of XRF and geochemical log determinations of sulfur, for the seven intervals of Table 1. See Figure 3 for explanation.

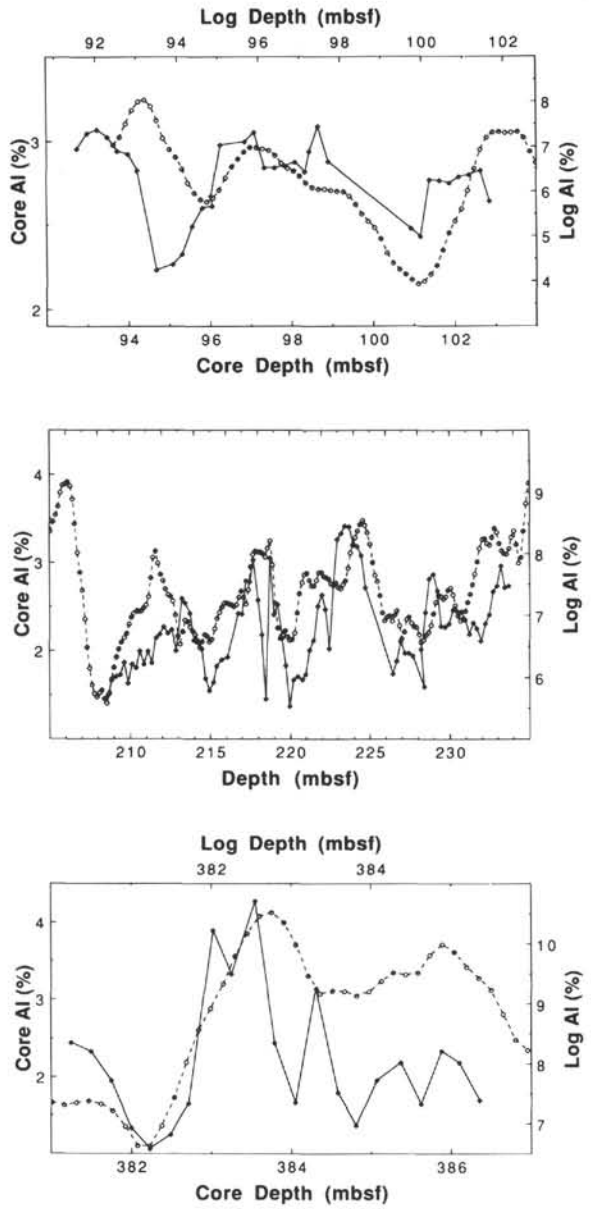

Figure 9. Comparison of XRF (solid lines) and geochemical log (dashed lines) determinations of aluminum, for the first three intervals of Table 1.

Aluminum concentrations (Fig. 9) are independent of the processing procedures used to refine GST elements. The aluminum clay tool is a tool very recently developed by Schlumberger, obtained by ODP partly because ODP provides a fruitful environment for testing its reliability. It is claimed to directly determine volume percent aluminum. However, at Site 723 the range of Al log values is much too high, and average Al log values are too high by a factor of 2–4. In view of the tool's demonstrated ability to reliably capture the character of small variations in formation aluminum, further calibration of the tool is certainly warranted. We cannot conclude on the basis of only one site that the log always overestimates formation aluminum concentrations.

With a combination of geochemical logs and a few XRF samples from the same site, one can greatly improve the geochemical log accuracy by calibrating the logs. Such a calibration is clearly warranted for the three sites of this study. However, it

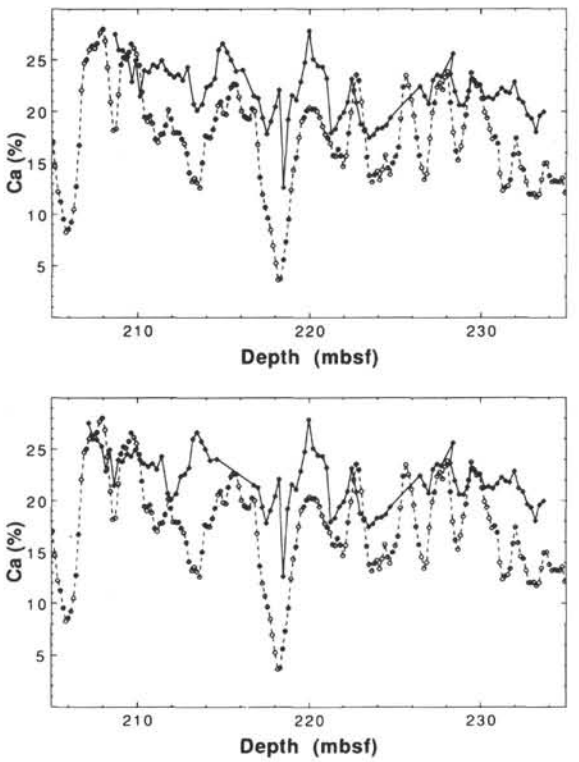

Figure 10. Comparison of XRF (solid lines) and geochemical log (dashed lines) determinations of calcium, for interval 2 of Table 1. Bottom: using the ODP convention of "hanging" core recovery from the top of the cored interval leads to a systematic mismatch of XRF and log character above 216.5 mbsf. Instead of assuming that incomplete core recovery is confined to the bottom of the cored interval, the top figure assumes that missing core was from the top of the cored interval.

is beyond the scope of the present study, and ideally it should be undertaken only after alternative processing schemes for GST data are compared, in order to reduce GST partitioning problems.

INTER-ELEMENT VARIATIONS

Examination of inter-element variations within both the XRF and log datasets offers a second method of evaluating geochemical log quality. This approach avoids a perennial problem of overlays of logs and core data as a function of depth: uncertain and variable depth shifts between cores and logs. It also reduces the problem of comparing character of log and XRF data, when the two datasets have different means and standard deviations (this difference does not affect the correlation coefficients of Table 5). A disadvantage of the method that we will use is that it does not consider the magnitude of elemental variances and whether they are much lower or higher than nominal log resolving power.

We applied principal components analysis to the XRF abundances of Ca, Si, Fe, Ti, K, and (at Site 723) Al. We chose these elements because they are the same ones available from logs, with one exception. We excluded sulfur, because XRF analyses show that it often moves independently of the other elements and because the XRF concentrations are far below the nominal S log resolution. We extracted principal components using the correlation matrix, effectively standardizing each element. For our purposes, this technique is much more appropriate than the alternative method which weights (or loads) components according to variance and which is therefore greatly dominated by calcium. XRF principal components were calculated for each of

the seven intervals; as for the correlation coefficients previously described, we excluded the first four measurements from interval 1 and first three measurements from interval 3, so that XRF and log data were available for exactly the same intervals. Geochemical log principal components were independently determined for the seven intervals. The first two principal components for both the XRF analyses and log analyses are shown in Table 6.

For XRF data, the first principal component is very strong and consistent throughout the seven intervals, accounting for 84.6%–99.6% of the covariance of the 5–6 analyzed elements. Although identification of a principal component with a physical mechanism can be hazardous, there is no doubt that the first principal component here is caused by calcite dilution. Calcium is opposite in sign to all other elements, and we see loadings for all of the elements that are near the perfectly equal ideals of 0.408 for intervals 1–3 (6 variables) and 0.447 for intervals 4–7 (5 variables). Because these principal components are effectively based on standardized variables rather than raw data, a given change in the dominant component Ca causes identical changes of opposite sign in all other components.

The second XRF principal component is more surprising and interesting. Although accounting for only 0.2%–13.2% of the covariance, it is very consistent among the seven intervals by principal component standards. This component is a silicon dilution effect, attributable to quartz or opaline silica. Silicon is the most highly loaded of the variables, and it is opposite in sign to the other variables (except occasionally to Ti). The contributions of Ti, Fe, and Al vary somewhat between intervals and are not particularly well defined, but Ca and K are relatively consistent. Note that this is not simply a variation in relative proportions of the two dominant elements Ca and Si. Instead the first two principal components indicate that most mineralogical abundance changes are in the relative proportions of calcite and combined "other" minerals (first principal component), but occasionally there is a quartz influx (second principal component). The same conclusion can be inferred from crossplots. Figures 11–13 show crossplots for the three sites (combining intervals within each site), illustrating both calcite dilution and occasional excess Si. We note, however, that the second principal component at Site 731 may be more complex than a simple quartz component; there Si and Ti are positively correlated (Table 6), and the turbidites of interval 7 have a particularly complex mineralogy (Prell, Niitsuma, et al., 1989).

The percent of variance accounted for by the first principal component is highest (99.6%) in interval 6, where the highest calcite concentrations are found (Table 5). However, the first principal component is not affected by total calcite concentration, and its relative strength in interval 6 probably results from a weak second principal component in the carbonates of Site 731, the most pelagic of the seven intervals.

The sum of the two principal components accounts for 97.4%–99.8% of the covariance of XRF elements included in this analysis. Thus principal components analysis makes very strong predictions about the inter-element relations expected among geochemical log elements.

Principal components analysis of the geochemical logs (Table 6) indicates substantially different patterns than the preceding analysis of XRF data, though the analyzed elements and depth intervals are identical. The first principal component is less than half the strength of the first XRF principal component. It is recognizably calcite dilution, consistently loaded on

Table 6. Principal components analysis.

Top depth	92.74	208.65	381.25	178.55	247.75	299.53	341.60
End depth	102.85	233.68	386.10	182.80	277.35	308.50	360.15
Number	30	93	17	18	122	30	59
X-ray diffraction							
%	93.1	84.6	93.6	97.4	96.4	99.6	93.2
Ca	0.406	0.401	0.408	0.452	0.449	0.447	0.460
Si	−0.412	−0.338	−0.380	−0.435	−0.440	−0.448	−0.448
K	−0.415	−0.420	−0.410	−0.450	−0.450	−0.446	−0.442
Ti	−0.417	−0.429	−0.416	−0.448	−0.446	−0.447	−0.450
Fe	−0.386	−0.432	−0.420	−0.451	−0.452	−0.447	−0.436
Al	−0.413	−0.422	−0.413				
%	4.4	13.2	6.1	2.3	2.2	0.2	5.3
Ca	0.280	0.461	0.408	0.110	0.284	0.459	0.199
Si	−0.427	−0.718	−0.714	−0.838	−0.746	−0.341	−0.473
K	0.269	0.315	0.386	0.275	0.324	0.778	0.485
Ti	−0.099	0.255	0.241	0.356	0.444	−0.172	−0.381
Fe	0.784	0.152	0.109	0.289	0.264	0.200	0.597
Al	−0.203	0.315	0.323				
% 1st + 2nd	97.4	97.9	99.7	99.7	98.6	99.8	98.5
Geochemical logs							
%	39.9	41.8	49.1	42.9	47.1	40.7	48.6
Ca	0.452	0.571	0.568	0.650	0.568	0.690	0.470
Si	−0.370	−0.586	−0.395	−0.600	−0.436	−0.469	−0.438
K	0.444	−0.254	−0.412	0.225	0.420	0.005	0.473
Ti	−0.493	−0.057	−0.386	−0.390	−0.397	−0.543	−0.344
Fe	−0.445	0.250	−0.323	0.127	0.390	−0.094	0.500
Al	0.142	−0.447	−0.313				
%	30.6	24.2	24.5	33.8	24.2	34.7	23.8
Ca	0.516	0.291	0.152	0.216	0.281	0.116	0.302
Si	−0.507	−0.008	0.449	0.171	0.538	0.124	−0.658
K	−0.416	−0.065	0.312	−0.580	−0.268	−0.694	−0.221
Ti	0.007	−0.734	0.316	−0.441	−0.708	0.153	0.609
Fe	0.403	−0.580	−0.538	−0.630	−0.240	−0.683	−0.236
Al	−0.376	0.189	−0.536				

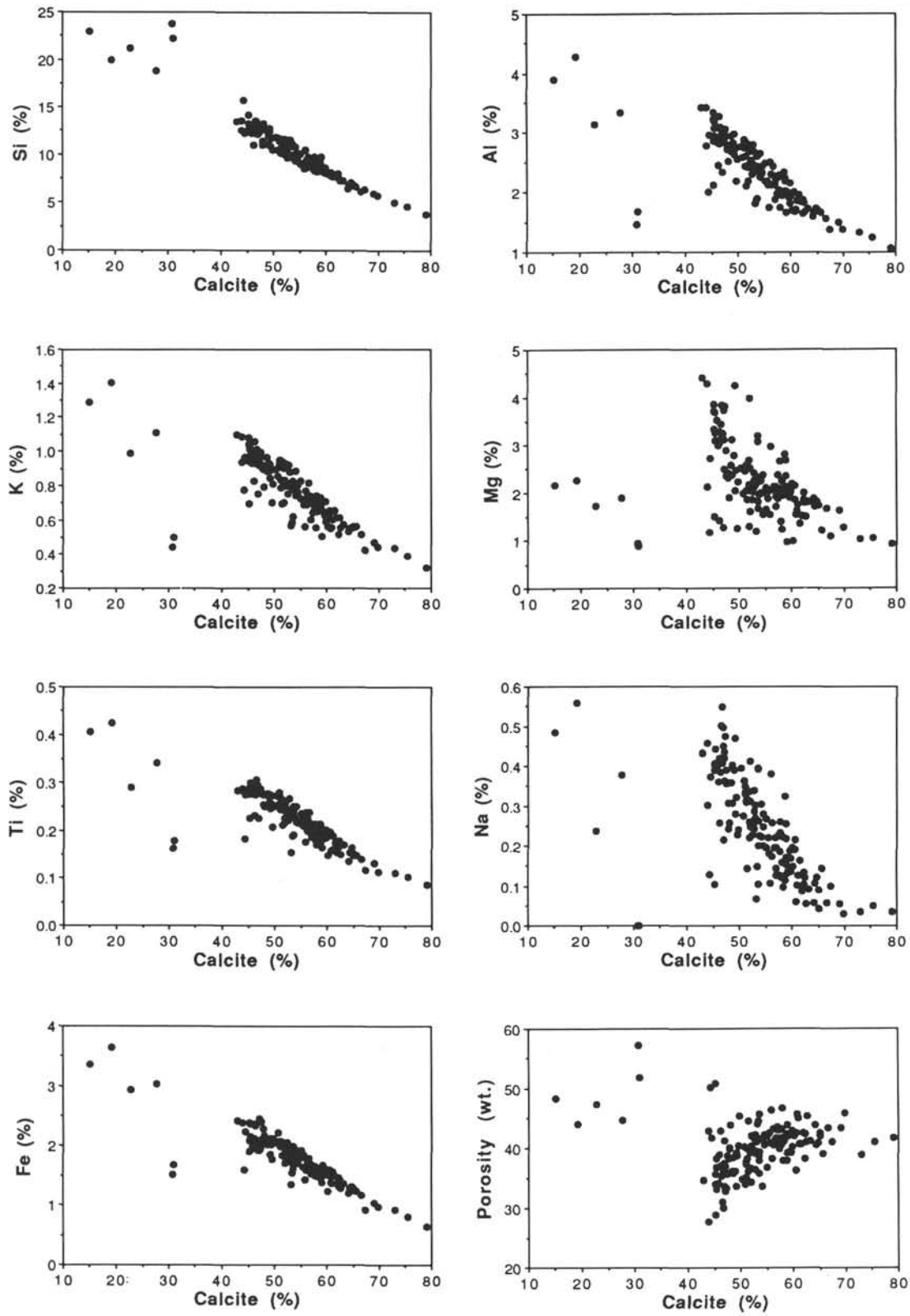

Figure 11. XRF element concentrations at Site 723, plotted as a function of XRF calcite percentage. Note the strong calcite dilution pattern for Si, K, Ti, Fe, and Al, with occasional discrepant points indicative of quartz dilution. The poor correlation of porosity and calcite suggests that our procedure of repartitioning all chlorine character to other logged elements is unlikely to create an artificial correlation between calcium and other logged elements.

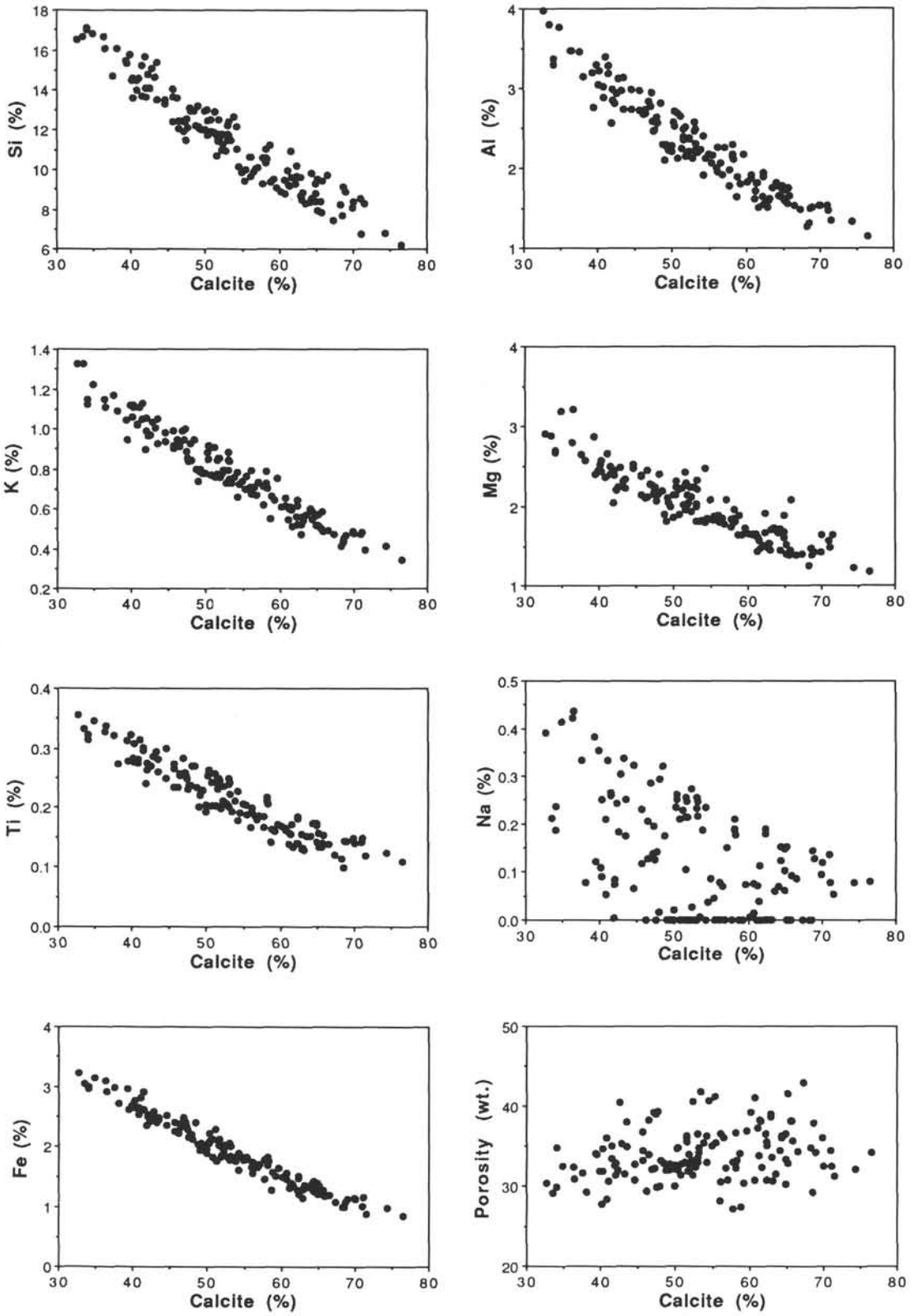

Figure 12. XRF element concentrations at Site 728, plotted as a function of XRF calcite percentage. Note the strong calcite dilution pattern for Si, K, Ti, Fe, Al, and Mg, with no obviously discrepant points indicative of quartz dilution. The poor correlation of porosity and calcite suggests that our procedure of repartitioning all chlorine character to other logged elements is unlikely to create an artificial correlation between calcium and other logged elements.

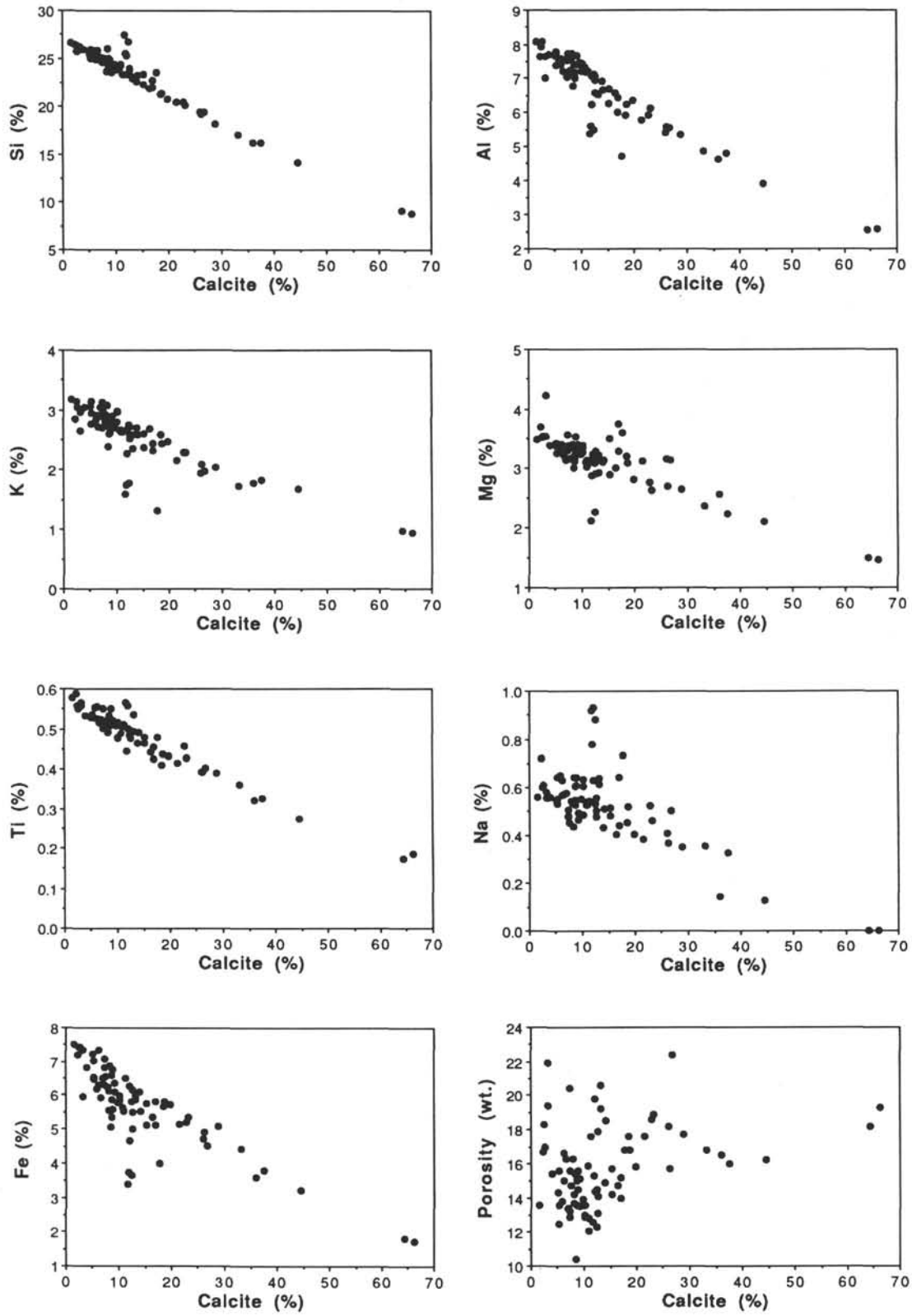

Figure 13. XRF element concentrations for the interval 340–450 mbsf at Site 731, plotted as a function of XRF calcite percentage. Note the strong calcite dilution pattern for Si, K, Ti, Fe, Al, and Mg, with occasional discrepant points indicative of quartz dilution. The poor correlation of porosity and calcite suggests that our procedure of repartitioning all chlorine character to other logged elements is unlikely to create an artificial correlation between calcium and other logged elements.

+Ca, -Si, and -Ti. This pattern indicates that real silicon and titanium variations are in the Si and Ti logs, a conclusion previously reached on the basis of element plots vs. depth for Si, but only tentatively concluded previously for Ti. Some inverse correlation between the dominant elements Ca and Si is introduced by the oxide normalization, but this effect cannot entirely account for the pattern seen here, because the inverse correlation is present, though weaker, before oxide normalization.

Only interval 3 shows the full calcite dilution pattern of positive Ca in the first principal component and negative loading for every other element. This interval also has the highest percentage of total covariance attributable to the first principal component (49.1%). K and Fe, which we previously inferred were poorly resolved by the logs in these intervals, give variable results in the first principal component and are often even positively correlated with Ca. Al loading for the first principal component is inversely correlated with Ca for intervals 2 and 3 and near zero but positively correlated for interval 1. This pattern is quite consistent with the Al vs. depth plots, in which we saw a good match to XRF in intervals 2 and 3 but only a fair match for interval 1 (which had Al variation far below the nominal resolving power of the logging tool).

If one calculates principal components from only the three logs Ca, Si, and Ti for each interval, the first principal component is again calcite dilution, accounting for 59%–70% of the covariance. Compared to the 88.5%–99.8% result from an XRF analysis of the same three elements, we may conclude that about two thirds (59%–77%) of the observed log variations in Ca, Si, and Ti is real detection of lithologic variation and about one third is noise. Calcium consistently has the heaviest loading in this first log principal component and therefore the highest signal-to-noise ratio; titanium usually has the lowest and contributes most to the combined noise of the three elements.

The second principal component for the geochemical logs accounts for 24%–35% of the covariance (Table 6) and is not much weaker than the first principal component. Its physical origin is obscure. It appears to pick up the effect of Ca dilution on K and Fe, since these elements are negatively loaded with respect to Ca in six of the seven intervals. However, only the portion of Ca log variations that is real calcite dilution and is also uncorrelated with log Si and Ti variation could be present in this second principal component. With loadings varying from interval to interval, it is not possible to assess the extent to which this component reflects calcite dilution, partitioning problems, and other systematic log errors.

CONCLUSIONS

The marly nannofossil chalks of Sites 723, 728, and 731 exhibit substantial geochemical variability at scales of 2–10 m. X-ray fluorescence analysis, based on high-resolution sampling of seven intervals, demonstrates that calcite dilution is the primary source of this variability; occasional quartz influxes are also detected. The geochemical logs Ca, Si, and Ti detect the calcite dilution with sufficient precision to permit interpretation of high-frequency variations in calcite content for intervals with no XRF data but with openhole geochemical logs—nearly the entire hole below 56–92 mbsf at the three sites.

Our comparisons of 398 XRF analyses with geochemical logs indicates that the reliability of geochemical logs varies substantially, within short intervals and particularly between sites. In general, the geochemical logs are capable of detecting changes in formation geochemistry that are larger than the following thresholds: 2% for Ca, 2%–6% for Si, 0.5%–1% for K, 0.1% for Ti, 0.5% for Fe, and 0.4% for Al.

Accuracy of geochemical log percentages requires both the full suite of geochemical logs and a log of photoelectric effect. We obtained this full suite only at Site 723; even there, we were prevented from determining Mg and thereby improving accuracy of the other geochemical logs by an unknown problem in the log of photoelectric effect. Without the full suite, we can make only first-order estimates of elemental percentages. These estimates yielded reasonable accuracy only for Ca and Si. Thus the character of geochemical logs is often more reliable than their magnitudes.

Both the processing of these geochemical logs and the comparison of them to XRF data suggest several ways in which the reliability of ODP geochemical logs could be increased. First, as already mentioned, ideally both the full suite of geochemical logs and a photoelectric effect log should be obtained. Second, a reliable caliper log would improve the NGT K log and thereby also improve GST K repartitioning. Third, improved partitioning of the GST spectra is needed. A boron sleeve to reduce Cl counts may help, the improved NGT K log will help, and further reprocessing experiments on the Leg 117 geochemical logs could lead to improved partitioning coefficients. We note that ODP does now have a reliable caliper and a boron sleeve for the GST. Thus geochemical logs obtained after Leg 125 should be examined to evaluate whether or not the quality of geochemical logs is now higher than we found for Leg 117.

ACKNOWLEDGMENTS

This project was made possible by Lamar Hayes, who obtained excellent core recovery on ODP Leg 117; the shipboard scientific and technical parties; samples provided by the Ocean Drilling Program; the highly efficient XRF analytical facilities of Oregon State University; and the U.S. Science Advisory Committee, grant TAMRF P.O. 20167. The U.S. Science Program associated with the Ocean Drilling Program is sponsored by the National Science Foundation and the Joint Oceanographic Institutions, Inc. Any opinions, findings and conclusions expressed in this publication are those of the authors and do not necessarily reflect the views of the National Science Foundation, the Joint Oceanographic Institutions, Inc., the Texas A&M University, or Columbia University.

REFERENCES

Anderson, R. N., Dove, R. E., and Pratson, E., in press. The calibration of geochemical well logs in basalt, granite, and metamorphic rocks; and their use as a lithostratigraphic tool. *Geol. Soc. London.*

Chapman, S., Colson, J. L., Flaum, C., Hertzog, R. C., Pirie, G., Scott, H., Everett, B., Herron, M. M., Schweitzer, J. S., La Vigne, J., Querein, J., and Wendlandt, R., 1987. The emergence of geochemical well logging. *Tech. Rev.,* 35:27–35.

Herron, M. M., 1986. Mineralogy from geochemical well logging. *Clays Clay Miner.,* 34:204–213.

Hertzog, R., 1979. Laboratory and field evaluation of an inelastic-neutron-scattering and capture gamma ray spectroscopy tool. *Soc. Pet. Eng., Pap.* 7430.

Herzog, R. L., Colson, B., Seeman, M., O'Brien, H., Scott, D., McKeon, P., Wraight, J., Schweitzer, J., and Herron, M., 1987. Geochemical logging with spectrometry tools. *Soc. Pet. Eng., Pap.* 16792.

Lock, G. A., and Hoyer, W. A., 1971. Natural gamma ray spectral logging. *Log Analyst,* 12:3–9.

Lyle, M., Heath, G. R., Pisias, N., and Muehlhausen, L., 1987. Sedimentary sources and diagenesis in the Pacific Ocean through the mapping of sediment chemical compositions. *Eos,* 68:470. (Abstract)

Prell, W. L., Niitsuma, N., et al., 1989. *Proc. ODP, Init. Repts.,* 117: College Station, TX (Ocean Drilling Program).

Schlumberger, 1988. *Trans., Inter. Spectroscopy Geochem. Symp.,* Ridgefield, CT (Schlumberger-Doll Res.).

Scott, H. D., and Smith, M. P., 1973. The aluminum activation log. *Log Analyst,* 14:3–12.

Serra, O., Baldwin, J., and Quiren, J., 1980. Theory, interpretation and practical applications of natural gamma-ray spectroscopy. *Trans. SPWLA 21st Annu. Logging Symp.,* Q1–Q30.

Date of initial receipt: 26 September 1989
Date of acceptance: 25 July 1990
Ms 117B-174